Manuscript File

Click here to view linked References

https://doi.org/10.1016/j.tws.2021.108158

This is the Pre-Published Version.

# Shape memory alloy plates: Cyclic tension-release performance, seismic applications in beam-to-column connections and a structural seismic demand perspective

Xuhong Zhou[a, b], Ke Ke[a, b, c, *], Michael CH Yam[d, e], Qingyang Zhao[c], Yun Huang[c], Jin Di[a]

[a] *School of Civil Engineering, Chongqing University, Chongqing, China*

[b] *Key Laboratory of New Technology for Construction of Cities in Mountain Area (Chongqing University), Ministry of Education, Chongqing, China*

[c] *Hunan Provincial Key Laboratory on Damage Diagnosis for Engineering Structures, Hunan University, Changsha, China*

[d] *Department of Building and Real Estate, The Hong Kong Polytechnic University, Hong Kong, China*

[e] *Chinese National Engineering Research Centre for Steel Construction (Hong Kong Branch), The Hong Kong Polytechnic University, Hong Kong, China*

**Abstract:**

This study examined the hysteretic behaviour of commercial Shape Memory Alloy (SMA) plates to promote their seismic applications in beam-to-column energy dissipation connections, and the research focus was given to the cyclic tension-release behaviour. Based on a series of SMA plate specimens, the investigation was commenced by examining the thermal characteristics, and the phase transformation behaviour of the SMA plates was characterised. Subsequently, cyclic tension-release tests of the SMA plates were conducted in the laboratory at room temperatures, and multi-phase tests considering varied loading protocols were carried out. It was observed that the self-centring capability of the SMA plates was comparatively less encouraging than bars and wires examined in the literature, whereas training cycles enabled stabilisation of the behaviour of the specimens by producing a newly recentring strain range with increased post-yield behaviour and decreasing martensite transformation stress. However, the energy dissipation of the SMA plates was reduced after experiencing the training protocols. Following the test programme, detailed numerical models of novel beam-to-column energy dissipation connection equipped with SMA plates were developed, and the feasibility of exploiting the cyclic behaviour of SMA plates was confirmed. Nonlinear spectral analyses of single-degree-of-freedom (SDF) systems representing structures were analysed to examine the influence of the structural hysteretic parameters on the structural inelastic demands quantified by strength reduction factor, and the influence of hysteretic parameters of the SMA plates on the structural seismic demand was characterised.

**Keywords:** shape memory alloy plate, cyclic behaviour, seismic engineering, dynamic analysis

Corresponding author. kerk.ke@outlook.com, keke@hnu.edu.cn



© 2021. This manuscript version is made available under the CC-BY-NC-ND 4.0 license https://creativecommons.org/licenses/by-nc-nd/4.0/

## 1. Introduction

In the recent decades, research communities and practitioners have developed a full-fledged ductility-based seismic design methodology for structures based on the "life-safety" objective. Nevertheless, recent seismic loss estimations [1] showed that inelasticity of members and connections of a conventional ductile structure could be triggered in rapid succession under earthquake actions, and post-earthquake structural damages and significant residual deformations were expected, leading to long-time occupancy suspension and costly repair works.

Hopefully, research advances of "self-centring" technology showed that it is possible to achieve both energy dissipation and rapid rehabilitation for seismic resistant structures. In parallel with the newly emerged structural-based technologies that produce self-centring behaviour with post-tensioned cables [2-7], the material-based technology motivated by the application of Shape Memory Alloy (SMA) [8-10] is also pursued by the research community. SMA is a smart metal with two extraordinary characteristics, namely the shape memory effect (SME) and the superelastic effect (SE). These two noteworthy features enable the SMAs to restore the deformed shapes to their undeformed shapes upon either heating (i.e. the SME) or unloading (i.e. SE), thereby realising the self-centring behaviour and dissipating energy during the loading and unloading process, as schematically shown in Fig. 1a. These extraordinary characteristics make SMAs economically viable. Due to a significant decrease of the SMA material price over the recent decades [8, 11] and increasing applications of the novel material in the biomedical, commercial and aerospace industries [11], it is reasonable to anticipate further room for price concessions in the

foreseeable future with continuously improved metallurgic technologies.

Recently, beam-to-column energy dissipation connections equipped with SMA bars/bolts are in the spotlight. For instance, Ocel et al. [12] modified the conventional welded flange-bolted web connection and replaced the welded connection in the flange area by SMA bars. Alternatively, Sepúlveda et al. [13] developed a modified end-plate bolted connection by replacing the bolts with superelastic SMA. Ma et al. [14] illustrated numerically the feasibility of using superelastic SMA bolts in beam-to-column connections. Yam and colleagues [15-17] investigated the behaviour of a series of stiffened extended end-plate (SEE) connections equipped with SMA bolts (Fig. 1b). The test results showed that the SEE connections equipped with SMA bolts could develop moderate energy dissipation capability and desirable self-centring behaviour under cyclic loading. Speicher et al. [18] and Wang et al. [19, 20] also conducted research works on various types of beam-to-column connections equipped with superelastic SMA bars/tendons. It is worth noting that in order to eliminate potential fracture over the threaded area of the SMA bars/bolts [15], the net threaded area of the bars/bolts should be sufficiently larger than the shank area. Moreover, the cyclic response of the beam-to-column connections equipped with SMA bolts may be influenced by the pre-strain in the SMA bolts, which requires much effort to control during installation. However, the limitations as discussed above may be overcome by using SMA plates. In fact, the rationale of developing novel energy dissipation components made from SMA plate element (e.g. SMA angles and U-shaped dampers) for seismic applications has been justified in the literature [21-24], whereas only the cyclic behaviour of the energy dissipation components was emphasised. In parallel with test

works, there were also several pilot numerical studies on applying SMA plates in beam-to-column connections of steel frames for resisting seismic actions [25-27]. However, more experimental studies are needed to substantiate the use of SMA plates in seismic resistant structures, particularly for SMA plates subjected to axial loading scenarios.

In light of the above, this research aims to offer further insights into cyclic performance of SMA plates to promote their seismic application. An experimental study was conducted to explore the hysteretic behaviour of commercial superelastic SMA plates, and the emphasis was given to the cyclic "tension-release" behaviour of SMA plates in a moderate strain range (below 4%). Specifically, the present study focused on SMA plates under cyclic tensile strains. The thermal characteristics, the transformation temperatures and their influence on the mechanical behaviour of SMA plates were also characterised using Differential Scanning Calorimeter (DSC). The mechanical properties of the SMA plates were carefully examined. The influence of training cycles which contributed to stabilising the behaviour of the alloy was explored, and the cyclic mechanical characteristics of the SMA plates after training was compared with that before training. Following the test programme, a numerical study was conducted to confirm the effectiveness of applying SMA plates in novel energy dissipation beam-to-column connections applicable to steel frames. Lastly, the seismic demands of low-to-medium rise structures equipped with superelastic SMA plates in the energy dissipation connections were examined using spectral analyses of equivalent single-degree-of-freedom (SDF) oscillators based on an ensemble of earthquake ground motions to demonstrate the potential of the SMA plates in improving the structural seismic behaviour.

## 2. Experimental programme

### *2.1. Material characteristics*

The SMA plates examined in the current work were made of commercial NiTi-based SMAs, and the atomic percentage of nickel was 50.95%. The specimens were ordered from Beijing Jiyi Corporation. According to the material supplier, the raw material was melted in an induction furnace and then worked into initial cast ingots with an approximate thickness of 40 mm. Following a hot-work process, a SMA ingot was eventually cold-worked to a designed thickness of 4 mm. Subsequently, the SMA plates were further heat-treated to achieve improved mechanical characteristics. It is worth mentioning that the annealing process contributed to developing precipitation of Ti3Ni4, which may appreciably affect the behaviour of the material. In particular, the presence of the Ti3Ni4 precipitates contributes to enhanced mechanical behaviour of SMA by facilitating the martensitic transformation and preventing plastic flow in the adjacent austenite matrix [28-31].

As for the annealing process, all the SMA plates were placed in an electrical furnace with varied temperatures and durations to achieve different austenite finish temperatures according to the supplier, and the information on the nominal austenite finish temperatures provided by the supplier is illustrated in Table 1. The nominal austenite finish temperature ($A_f$) of all SMA plates was below 20 ℃, and hence the plate specimens were expected to exhibit superelastic behaviour at room temperatures. Nevertheless, as the heat-treatment strategy is a trade secret, the detailed annealing protocols were not further disclosed by the supplier. Note that as the primary objective of the current study was to explore the cyclic tension-release behaviour of commercial superelastic SMA plates and examine the

practical feasibility in resisting seismic actions, the ideal annealing strategy was not within the scope of the current paper. However, to shed insightful lights on the thermal-mechanical characteristics of the material, the transformation temperatures of the SMA plates were examined in the test programme, which will be discussed in later sections.

### *2.2. Plate specimens*

Fig. 2 illustrates the designed geometry of NiTi SMA plates, including SMA coupons and a prototype plate that can be applied to realistic beam-to-column connections of a steel frame. In particular, Type A specimen (Coupon specimen) was designed according to ASTM 370 [32], and a gauge length of 50 mm was considered. As for Type B specimen, it was designed to accommodate a realistic connection in a steel frame. Specifically, the plate was cut from a rectangular plate with the designed dimension of 550 × 80 × 4 (unit: mm), and the reduced section was designed considering strength reduction of 43.8% to limit inelastic actions in the gauge length. The measured geometric information on the plate specimens was summarised in Table 1. According to the product category information offered by the supplier, specimen PA-0, PA-1, PA-2, PA-3, PA-4, PA-5, PA-6 and PB were normal superelastic SMA, whereas specimen PA-7 and PA-8 were categorised as "high strength superelastic SMA".

### *2.3. Identification of transformation temperatures*

For the SMA material, the transformation from austenite to martensite is defined as

151 "forward transformation", and the transition from martensite to austenite is "reverse
152 transformation". Therefore, four temperatures including the martensite start temperature
153 ($M_s$), the martensite finish temperature ($M_f$), the austenite start temperature ($A_s$) and the
154 austenite finish temperature ($A_f$), which feature the critical transformation phases of the
155 material can be identified (Fig. 1). Note that these transformation temperatures are
156 essential thermal parameters which appreciably affect the behaviour of SMA. Ideally, the
157 SMA exhibits superelastic effect at temperatures above $A_f$, whereas it shows full shape
158 memory effect at the temperature below $M_f$.

159 To provide in-depth insights into the thermal-mechanical characteristics of the SMA
160 plates, Differential Scanning Calorimetry (DSC) method was utilised to examine the
161 transformation temperature of the specimens. To obtain the transformation temperatures,
162 sample material cut from the specimens was placed in a Differential Scanning Calorimeter
163 (Fig. 3) to undergo a cooling-heating cycle with temperature changing (10 ℃ per minute),
164 and evident heat flows could be captured by the testing machine when the material
165 experienced phase transition, offering an indication of the corresponding transformation
166 temperatures.

167 Fig. 4 demonstrates the DSC test responses of samples extracted from plate specimens,
168 and the phase transformation temperature may be identified. It is worth noting that the shape
169 of DSC response curves may be affected by various factors such as heat-treatment strategy,
170 material chemical composition and mechanical deformation history [28]. In general, for
171 DSC response curves with two successive peaks, the SMA material experienced an
172 intermediate phase defined as rhombohedral phase between the austenite and martensite

phase [28]. In contrast, a single peak in the DSC test curves implied that the alloy underwent transformation without going through the rhombohedral phase. It can be seen that most alloy samples (except for sample of the high strength plates PA-7 and PA-8) underwent two-stage transformation in the cooling cycle (Fig. 4a), and the forward transformation generally initiated at various temperatures ranging from -20 to 40 ℃ owing to the different heat-treatment protocols adopted by the suppliers. However, the entire transformation was accomplished at a temperature above -80 ℃. As for the heating cycle, an evident peak can be extracted from test responses (heating cycle) of specimen PA-0, PA-2, PA-3, PA-4, PA-5 and PA-6, and the reverse transformation for these coupons was generally finished at the temperature close to 20 ℃. The DSC results of Type B specimen PB (i.e. the dog-bone-shaped plate) are shown in Fig. 4b, and similar features were characterised. However, it is worth noting that the DSC response curves of the high strength specimen PA-7 and PA-8 did not experience pronounced peaks in the heating and cooling cycles. This phenomenon might be attributed to different thermal aging processes and content of cold-worked fractions in the plate, as echoed by research works focusing on thermal-mechanical properties of SMA wires [33].

### *2.4. Cyclic tension-release tests*

The plate specimens were axially loaded by a servo-hydraulic dynamic system (i.e. INSTRON 8803) considering cyclic tension-release loading scenarios, and the test rig is illustrated in Fig. 5. The applied load was recorded by built-in load cells, and hence the engineering stress was obtained by dividing the load by the measured cross-section area.

The strain of the specimen was recorded by an extensometer mounted on the plate specimens. It is worth noting that the accuracy of the measured data by the extensometer was confirmed by readings of the strain gauges mounted on both sides of the specimen before the formal test. Recent research works on SMA plate elements [22, 24] show that the self-centring behaviour of SMA plates might not be as satisfactory as SMA wires [11, 28, 33] or bars [11]. Therefore, a tension-release loading protocol with incremental strain cycles (0.5%, 1.0%, 2.0 %, 3.0% and 4.0%) as "Phase 1" of the test programme was firstly applied, and two cycles were included for each amplitude. To examine the influence of the training scheme on the cyclic tension-release performance of the plate specimens, selected Type A specimens (i.e. PA-2, PA-3, PA-4 and PA-5) and Type B specimen (i.e. specimen PB) after being loaded to a strain of 4% were further trained in "Phase 2" considering a constant strain amplitude subsequently. In particular, PA-2 and PB were subjected to a constant strain amplitude of 4%. PA-3 was subjected to training cycles with a constant strain of 6%, and a protocol with a constant strain of 5% was applied to PA-4 and PA-5. For specimen PA-2 and PA-3, the training was terminated when the residual strain was stabilised (i.e. the residual strain difference between two cycles was below 0.1%). For specimen PA-4, PA-5 and PB, ten cycles were employed. After the training protocol, Type A specimens (i.e. PA-2, PA-3, PA-4 and PA-5) further experienced incremental strain cycles until fracture as "Phase 3" of the test programme. Type B specimen PB was also re-examined after the training cycles, and the test was terminated when the maximum strain reached 4%. Two loading protocols for re-testing the specimens are shown in Fig. 6. For specimen PB, an additional cycle of 3.5% was added based on "Protocol 2". The

information about the re-test is also indicated in Table 1. For all test specimens, a strain-force hybrid control approach was used. In particular, when a specimen was subjected to tension, the strain control approach with a constant strain rate of 0.02%/s was employed, and a force control approach was subsequently incorporated in the unloading half cycle, in which the unloading rate was 0.2 kN/s. Thus, a quasi-static loading condition may be ensured. All the tests were conducted in a laboratory with the room temperature ranging from 23.5 to 25 ℃. Recalling the DSC test responses mentioned in the previous subsection, it was anticipated that most specimens exhibited superelastic behaviour.

## 3. Test results and discussions

### *3.1. Test results*

#### *3.1.1 Stress-strain responses (Phase 1 test)*

Stress-strain response curves of Type A specimens subjected to cyclic tension-release loading scenarios (till 4%) are shown in Fig. 7a. Most Type A plate specimens showed an evident transformation plateau, although the residual strain increased with load amplitude increasing. This phenomenon was defined as Transformation Induced Fatigue (TIF), which was characterised in other studies on commercial superelastic SMAs [28]. In general, the strain recoverability of the SMA plates was comparatively less satisfactory than bars and wires reported in the literature [11, 28, 33], and a residual strain close to 1% was sustained by the specimen PA-0, PA-2, PA-4 and PA-5 after experiencing a peak strain of 4%. This phenomenon implied that the microstructure of SMA plates (e.g. grain sizes, grain orientations, and precipitates) may be different from the SMA wires and bars. This is understandable as the rolling and production process of a SMA plate is different from

producing bars and wires due to different geometric features. However, more test evidence confirming the microstructure of the SMA plate may be in need. For PA-1 and PA-3 with a higher $A_f$ according to Fig. 4a, the recentring performance was further compromised as the residual strain exceeded 1.5% after the specimen was loaded to 4%. Type B specimen with a larger size exhibited features of typical superelastic SMA with a pronounced stress plateau, and a residual strain of 0.5% approximately was achieved when unloaded from 4%, which corresponded to the recovery rate close to 85%. In contrast, high strength specimen PA-7 and PA-8 reached a higher strength when inelasticity was triggered. It is also of great importance to note that the area covered by the hysteretic loop of specimen PA-7 and that by PA-8 was smaller than other specimens, and a "yielding plateau" was less pronounced than other SMA specimens. These phenomena could be attributed to the combined effects between the high content of cold-worked fraction in the plates and different annealing schemes, which were also observed in a work focusing on the behaviour of SMA wires [33]. In general, the cold-worked fraction may contribute to enhanced strength and recentring behaviour, whereas the energy dissipation could be compromised.

It is worth noting that the encouraging performance of superelastic SMA was generally characterised by an evident stress plateau and satisfactory recentring ability when SMA was applied in energy dissipation fuses. In particular, an evident stress plateau contributes to stabilising "yield strength" of the energy dissipation fuses to concentrate inelasticity, and the self-centring performance of SMA results in mitigation of post-earthquake residual deformations sustained in the energy dissipation elements. However, for the results shown

in Fig. 7, the SMA plates showed inconsistent behaviour. Thus, further training cycles leading to stabilisation of the SMA plates were conducted, which will be discussed in the next section.

*3.1.2 Training cycles (Phase 2 test)*

Fig. 8 presents the stress-strain responses of PA-2, PA-3, PA-4, PA-5 and PB subjected to training cycles after "Phase 1" test. Note that the training process employing load cycles was found to be a feasible solution to obtain steady-state hysteretic responses for SMA bars and wires [34, 35]. According to Fig. 8, it can be confirmed that the training loading protocol contributed to stabilising the hysteretic responses of the plate specimens, although certain degradation of the peak strength and energy dissipation was observed. In addition, the training cycles resulted in hysteretic behaviour alteration of the plate specimens. In particular, compared with the response curves in the "Phase 1" test showing an evident stress transformation plateau, the stress-strain response curves in the training cycles were transformed to typical leaf-shaped responses [33] with reduced energy dissipation. According to the stabilised hysteretic loops, the newly formed self-centring deformation spectrum of the plate specimens with minimised residual strain may be predicted, as indicated in the training cycles, which will be further examined in the results of "Phase 3" test. In addition, it is important to note that PA-3 entered the martensite hardening stage under the training cycles when loaded to 6%, and the hysteretic behaviour deterioration was pronounced. Thus, special caution should be exercised when developing the training scheme for SMA plates, and a significant strain which was found to be feasible for training SMA bars and wires [34, 36] may not apply to SMA plates.

285 *3.1.3 Stress-strain response (Phase 3 test)*

286 The stress-strain responses of the specimens from "Phase 3" test were extracted from the
287 result database, as shown in Fig. 9. Comparing the stress-strain responses in "Phase 1" and
288 "Phase 2" test, it can be seen that the stress transformation plateau of the specimens in
289 "Phase 3" was much less pronounced, and a significant "post-yield stiffness ratio" was
290 obtained when inelasticity was triggered. In general, encouraging self-centring behaviour of
291 the plate specimens in a certain deformation range was observed, and the strain spectrum of
292 the specimens showing excellent self-centring behaviour was in good agreement with that
293 characterised from response curves in the training cycles in "Phase 2" test (Fig. 8). Thus, the
294 training cycles may enhance the recentring ability, but the stress plateau might need to be
295 sacrificed due to the significant "post-yield stiffness ratio". The influence of this behaviour
296 change on the structural seismic performance will be further explored in a next section from
297 a structural seismic demand perspective. The test response of specimens (i.e. PA-2, PA-3,
298 PA-4 and PA-5) loaded to complete failure showed that the recentring ability of the plate
299 deteriorated rapidly after the strain going beyond the newly formed self-centring region. For
300 specimen PA-2 and PA-3 showing good ductility, significant increase in stress at high strain
301 levels induced by the martensite hardening was observed. Eventually, specimen PA-2 and
302 PA-3 failed by fracture in the gauge length at the strain level of 15.0 % and 13.0 %,
303 respectively. In contrast, the ductility of specimen PA-4 and PA-5 in the post-training stage
304 was much poorer than that of specimen PA-2 and PA-3, and the two specimens fractured at
305 the strain of 3.5 % and 5.0 % in "Phase 3" test in the transition region between the gauge
306 length region and gripping ends, respectively. It is significant and interesting to note that
307 both PA-4 and PA-5 had a lower $A_f$ compared with that of PA-2 and PA-3 according to Fig.

4, and hence special care may need to be taken when selecting the heat-treatment strategy to pursue the superelasticity of SMA plates, since the inelastic deformability of the material might also be affected.

### *3.2. Discussions of the test results*

#### *3.2.1 Strength and stiffness*

The martensite transformation stress of SMA plate specimens, which may be reckoned as the "pseudo-yield strength" of the plates, was extracted and plotted against the cycle numbers, and the results corresponding to various test phases are shown in Fig. 10. The strain amplitude corresponding to each cycle is indicated in the figure. The equivalent pseudo-yield strength is determined by the intersection point of the line quantifying the initial slope and the extension line along the path of the inelastic branch of each loading cycle, as shown in Fig. 10. In particular, the initial stiffness of the curve was quantified by the tangent stiffness of the material in a cycle, and the post-yield stiffness in the corresponding cycle was computed by the tangent line from the end point of the post-yield branch in each cycle. This method was also adopted by Fang et al. [28] in a study focusing on the behaviour of SMA cables. It is worth mentioning that the definition was actually based on bilinear idealisation of the test results, and the defined "yield point" and corresponding stiffnesses are nominal values. Nonetheless, these indicators can shed insightful lights on the mechanical behaviour of the material. It can be observed that for "Phase 1" and "Phase 2", the pseudo-yield strength decreased with increasing loading cycles. This phenomenon indicates that the strength degradation of SMA plates was induced by

330 both peak strain and the cumulative strain, echoing the test findings by Fang et al. [28] with
331 a focus on SMA wires and cables. In contrast, for specimens in "Phase 3", it was observed
332 that the equivalent pseudo-yield strength generally increased with increasing loading cycles
333 in the early stage (i.e. below 2%). These results imply that the behaviour of SMA plates was
334 stable in the newly formed self-centring deformation spectrum, and the increasing
335 equivalent pseudo-yield strength was due to the bilinear idealisation approach. However,
336 this trend was altered in the later stage with peak strain going beyond 2%, exhibiting the
337 strength degradation effect as characterised in "Phase 1" and "Phase 2".

338 The peak stress of the SMA plates in each cycle is also correlated with the cycle
339 numbers and strain amplitude, as shown in Fig. 11. In general, for specimens subjected to
340 incremental cyclic loading (i.e. "Phase 1" and "Phase 3"), the peak strength increased with
341 the strain amplitude, although the repetition of loading cycles at the same strain level
342 caused slight deterioration of the peak strength (Fig. 11a). According to the results of
343 training cycles ("Phase 2") as shown in Fig. 11b, it can be seen that the peak stress
344 deterioration was only evident in the first few cycles. Comparing the peak stress response
345 of "Phase 1" and "Phase 3", it is evident that the increasing trend of the peak strength in
346 "Phase 3" test was more pronounced, confirming the influence of the training protocols on
347 the behaviour of the SMA plates. Note that the similar observation was also characterised in
348 recent tests [34] focusing on SMA bars. However, it should be cautious to select a suitable
349 training scheme to avoid over-training, which will be discussed in later sections.

350 In addition, the different post-yield behaviour of the SMA plate specimens in various
351 phases was noticeable, and the post-yield stiffness ratio of the alloy in different phases is

correlated with loading cycles, shown in Fig. 12. To determine the post-yield stiffness ratio ($\alpha$) of each loading cycle (Fig. 12), the bilinear simplification as illustrated in Fig. 10a was first applied, and the ratio of the post-yield stiffness to the initial stiffness was finalised. In "Phase 1", the post-yield stiffness ratio generally decreased with load cycle numbers in the early stage, which was expected due to stress transformation. However, the opposite trend was characterised in late cycles at more significant strain levels, echoing the shape transformation of the hysteretic loops shown by Fig. 7. As for the post-yield behaviour of the selected specimens in "Phase 2", it can be seen that the training cycles may contribute to enhancing the post-yield behaviour of the material, which was further echoed by significant post-yield stiffness ratios of the specimens in "Phase 3". Note that a large post-yield stiffness ratio was found to be effective in producing more encouraging inelastic seismic responses, which was actively pursued by both research communities and practitioners. Thus, an applicable training protocol may help the SMA plates achieve the desirable feature.

*3.2.2 Residual strain evolutions*

The residual strain evolution of the SMA plate specimens in various loading phases is plotted against loading cycle numbers and the maximum strain amplitude, as presented in Fig. 13. The results of specimens in "Phase 1" (Fig. 13a) consistently showed that the residual strain increased with the maximum strain and cycle numbers. As for the selected specimens undergoing training cycles in "Phase 2" (Fig. 13b), it can be seen that the development of the residual strain was most evident for the first few cycles, and further repetition of the training cycles led to convergence of the residual strain. The effectiveness

375 of the training scheme was further verified by the residual strain evolution responses of the
376 SMA plates in "Phase 3", as illustrated in Fig. 13c. As can be seen, the development of the
377 residual strain was slow in the expected self-centring spectrum (Fig. 8), and the
378 encouraging self-centring performance of the SMA plates in the anticipated strain range
379 after training cycles was confirmed.

380

381 *3.2.3 Energy dissipation capacity*

382 To examine the energy dissipation capacity of the SMA plates as energy dissipation
383 elements, the energy dissipation of the SMA plates quantified by equivalent viscous
384 damping index [28] is presented in Fig. 14. The equation for calculating the index is
385 reproduced by

386 $$\xi = \frac{E_a}{4\pi E_e} \quad (1)$$

387 where $E_a$ = strain energy dissipation per load cycle quantified by the enclosed area of the
388 stress versus strain hysteretic loop; $E_e$ = strain energy of the corresponding linear elastic
389 element. The equivalent viscous damping generally increased with strain amplitude in
390 "Phase 1" owing to the fuller hysteretic loop. In contrast, the equivalent viscous damping
391 decreased with load cycle numbers in "Phase 2" as a result of material behaviour
392 degradation. In addition, the comparison between the equivalent viscous damping index of
393 "Phase 1" and "Phase 3" showed that although the enhanced self-centring performance of
394 the SMA plates in the post-training stage was ensured, trade-offs between energy
395 dissipation and self-centring behaviour may need to be made. Particularly for specimen
396 PA-3, behaviour deterioration was triggered due to the "over-training" effect in Phase 2,

and the viscous damping was greatly compromised. Therefore, it should be re-emphasised that the training protocol may need to be selected wisely.

*3.2.4 Further comments*

In light of the above, it may be seen that the cyclic tension-release behaviour of superelastic SMA plates is different from SMA bars and wires examined in the literature [11, 28, 36]. In addition, the post-training behaviour of the SMA plates could be altered, and the enhanced self-centring behaviour of the alloy was realised at the expense of energy dissipation. In cases where the specimens were "over-trained" and entered the martensite hardening stage, the deterioration of the energy dissipation was noticeable. Therefore, an applicable training scheme may be essential to achieve optimised behaviour of the superelastic SMA plates subjected to cyclic tension-release loading scenarios. In fact, the research community had confirmed the influence of the training protocol and strain amplitude on the behaviour of SMA wires and bars [34, 36-38] in previous works, whereas the optimised training scheme of SMA plates was not clearly examined due to insufficient test data. Therefore, a stepwise procedure based on coupon tests was proposed in the current study to determine the training scheme, which may result in delicate balance between self-centring capacity and energy dissipation ability of SMA plate elements.

**Step 1**: As a start point, prepare two coupons (i.e. Coupon A and B) corresponding to the SMA plate element, and apply an incremental loading protocol with increment of 1% (two cycles for each amplitude) to "Coupon A" till the martensite hardening stage (Fig. 15).

**Step 2**: Select a strain amplitude ($\varepsilon_a$ in Fig. 15) for conducting the training for Coupon A

based on the stress-strain responses obtained from Step 1, and the strain amplitude with a reasonable self-centring spectrum and encouraging energy dissipation may be preferable.

**Step 3**: Based on the preselected strain amplitude, conduct a trial training on coupon B with the selected constant loading protocol (i.e. amplitude $\varepsilon_0 + \varepsilon_a$ in Fig. 15, where $\varepsilon_0$ is the nominal residual strain determined from test responses of Coupon A), and the training may be terminated until the "nth" cycle, determined by the following criterion:

$$\left| \frac{\varepsilon_n - \varepsilon_{n-1}}{\varepsilon_{n-1}} \right| \leq \Theta \tag{2}$$

where $\varepsilon_n$ = residual strain of the specimen after the "nth" cycle; $\varepsilon_{n-1}$ residual strain of the specimen after the "($n$-1)th" cycle and $\Theta$ = convergence criterion. In general, a sufficiently small value of $\Theta$ may suffice. When the behaviour of the plate was stabilised, the newly formed self-centring strain range may also be obtained.

**Step 4**: Iterations may be needed to search for the optimised training protocol. Recalling that a significant strain may cause behaviour deterioration and permanent deformations were sustained by the material, it is necessary to keep the target strain below the threshold where evident martensite hardening is triggered. Then, train the SMA plate element using the developed training scheme derived from the test responses of the coupons. In this context, the optimised cyclic tension-release behaviour of the SMA plate element with an expected self-centring strain range ($\varepsilon_{sc}$ in Fig. 15) may be ensured. A flowchart illustrating the procedure is shown in Fig. 15.

## 4. Numerical investigations

### *4.1. Notion of self-centring connection equipped with SMA plates and prototypes*

A novel self-centring SMA connection was proposed as an application strategy of the SMA plates in steel frames. An overview of the novel connection is schematically shown in Fig. 16. In particular, the superelastic SMA plates connect the adjacent beam flanges using high strength friction grip bolts to resist the connection moment, and they could provide both the recentring and energy absorption capabilities for the connection at room temperatures, owing to the SE effect which allows recentring of the connection upon unloading. The shear force applied to the connection is resisted by the HS bearing bolts that connect the two end-plates welded to the beam webs. In addition, to eliminate the possible permanent axial deformation of the HS bolts due to the connection moment, superelastic SMA Belleville spring washers [17] are used along with the HS bolts to absorb the deformation. The deformation of the SMA Belleville spring washers also contributes to certain energy absorption capabilities of the connection. Therefore, it can be seen that the proposed novel connection is able to resist the applied connection moment using the SMA plates connected to the beam flanges and to resist the applied shear force using the HS bearing bolts with SMA washers connected to the web end-plates. Under both positive and negative moments, it is expected that the rotation centre of the connection is within the axis of flanges, and the SMA plates in the connection may be dominated by the tension-release action, and the compressive action of the plates may be minimised. The potential buckling issue of the end-plate edge (i.e. the plate connecting the SMA plate) could also be effectively eliminated using a force-based design approach, as the compressive force transferred from the SMA plates can be quantified based on force equilibrium. Note that the loading transfer mechanism of the proposed connection notion is similar to novel energy dissipation

connections equipped with various steel plates [39, 40] reported in the literature, whereas the proposed notion in the current study explored the potential of a delicate balance between self-centring capability and energy dissipation of the connection.

### *4.2. Modelling of SMA plates and the novel connections*

Software ABAQUS [41] was utilised to develop finite element (FE) models of the SMA plate and a prototype connection mentioned above to confirm the feasibility of making use of the cyclic tension-release behaviour the SMA plates in seismic resistant beam-to-column energy dissipation connections. As a start point, the behaviour of the plate specimen PB before and after the training protocol was simulated. In particular, PB was discretised by C3D8 elements with a mesh size of 3 mm, and a fixed boundary condition at both ends was adopted to reproduce the strong gripping restraints provided by the test machine. Auricchio's hysteretic model [42] was utilised to quantify the hysteretic parameters of the SMA. The essential material coefficients including the state transformation stresses, i.e. forward transformation start stress ($\sigma^{MS}$), forward transformation end stress ($\sigma^{Mf}$), reverse transformation start stress ($\sigma^{AS}$) and reverse transformation end stress ($\sigma^{Af}$), austenite elasticity ($E^{A}$), martensite elasticity ($E^{M}$), and Poisson ratios ($\nu^{A}$ and $\nu^{M}$), are indicated in Table 2, which were finalised following a trial-and-error process based on the test data. The FE prediction of the SMA plate in terms of stress-strain responses till the strain of 3% was compared with the test results, as shown in Fig. 17a, and the sufficiency of the modelling techniques for reproducing the responses of the SMA plate in the self-centring spectrum before and after training was verified. Note that in cases where the strain exceeds 3%, the residual strain would develop rapidly, and

Auricchio's model may not be applicable. However, modulation of the connection design (e.g. increasing the gauge length of the SMA plate or decreasing the beam depth) may be effective in controlling the strain level in the SMA plate, contributing to a stable self-centring deformation range of the connection. Similarly, the Auricchio's hysteretic model was employed to simulate the compression-release behaviour of SMA Belleville spring washers, and the material characteristics are also indicated in Table 2, which were determined based on test data provided by Fang et al. [17]. The sufficiency of the hysteretic parameters for reproducing the behaviour of SMA washers after training can be confirmed from the good agreement between the test responses and FE results shown in Fig. 17b.

On the basis of the verified model for reproducing the tension-release behaviour of SMA plates and compression-release behaviour of SMA Belleville washers, a case study on a prototype connection was conducted. The geometric information and detail of the connection is shown in Fig. 18a and Table 3. In the FE model of the prototype connection, the column and beam stub were simulated by "C3D8R" elements. "Hard contact" which may simulate the interaction among structural elements in the normal direction was assigned to all contacting surfaces. Concurrently, a "Penalty function" with the friction coefficient of 0.3 featuring the friction action of the contacting surfaces was used. It was assumed that no welding failure would occur, and the "Merge" option was utilised to model the welded junctions of the I-section beams and columns. The bilinear kinematic hysteretic material model dominated by von Mises yield criterion is used for the steel. Note that the sufficiency of the modelling techniques for simulating the behaviour of a steel connection equipped with SMAs has been verified in extensive works [16, 17]. The

prototype connections equipped with SMA plates considering material properties before and after training were subjected to cyclic loading scenarios, and the hysteretic responses are shown in Fig. 18b. Comparing the FE results of two connections, it is reconfirmed that the training scheme may enhance the "post-yielding" behaviour of the connection, but the energy dissipation capacity of the connection was sacrificed. The strain contours of the SMA plates ("Phase 3") arranged in both the top and bottom flanges at the maximum deformation of 4% drift (sagging) were extracted and shown in Fig. 18c. As can been seen, the SMA plates at the top flange was in tension with the maximum tensile strain below 3%, whereas the counterparts at the bottom flange were in slight compression and deformed elastically. There is also test evidence showing that slight compression in the elastic stage does not affect the tension-release behaviour of SMA according to a recent study [34]. Thus, in the numerical investigation, it was assumed that the material model of SMA is dominated by the tension-release action, and the minimal effect produced by the slight compression was neglected.

To examine the influence of SMA properties, the material parameters extracted from SMA bars examined by Fang et al. [17] were assigned to the SMA plates. For comparison, the conventional end-plate connection was also analysed, and the end-plate of the conventional connection was identical to that of the prototype connection to provide a comparable basis. To offer a direct comprehension of the hysteresis characteristics of different connections, the hysteretic responses of various connections are summarised in Fig. 18d in a normalised pattern (i.e. $M_n = M/M_u$, where $M$ is the connection moment and $M_u$ is the maximum connection moment till the rotation of 4%). For the SMA connection

assigned with the material model of SMA bars [17], the varied hysteretic response compared with the counterpart with SMA characteristics obtained in the current study (i.e. PB Phase 1) can be seen, and the sensitivity of the connection to the material properties is confirmed. In addition, the conventional connection shows fuller hysteretic response, whereas the residual deformation also increased rapidly with load drift increasing. The deformation modes of the prototype connection and the conventional end plate connection are shown in Fig. 18d. As can been seen, the prototype connection can concentrate the inelastic action in SMA plates.

### *4.3. Seismic demands from a structural perspective*

#### *4.3.1 Simplified structural model, demand quantity and earthquake motions*

To offer further insights into the effectiveness of applying the self-centring connections equipped with SMA plates in seismic resistant structures, nonlinear spectral analyses were conducted based on the single-degree-of-freedom (SDF) oscillators. As a reasonable idealisation, cyclic behaviour of a structure equipped with the novel self-centring connections may also be simplified by a bilinear flag-shaped hysteretic model [42], and the rationale of the SDF analogy for representing a structure was confirmed in the previous studies [43-47].

The idealised SDF oscillator and the essential quantities are shown in Fig. 19a. In particular, $F$ = base shear of the SDF system; $\delta$ = displacement of the SDOF system; $\alpha$ = post-yield stiffness ratio of the system; $\beta$ = ratio of the flag height to the yield force $F_y$ and $\mu$ = ductility of the system quantified by the maximum displacement $\delta_m$ to that of the yield

553 displacement $\delta_y$. In general, the nonlinear dynamic characteristics of a SDF oscillator
554 representing a structure equipped with the novel self-centring connections may be
555 quantified by nonlinear hysteretic parameters ($\alpha$, $\beta$ and $\mu$) and initial elastic dynamic
556 quantities of the system including mass ($M$), elastic period ($T$) and the damping ratio ($\xi$).
557 To demonstrate the sufficiency of the bilinear flag-shaped model for quantifying the
558 structural hysteretic behaviour, the hysteretic responses of the connection were further
559 idealised by the bilinear flag-shaped hysteretic model, as indicated in Fig. 18b. As can be
560 seen, the good agreement between the analysis results and model idealisation has
561 confirmed the applicability of the hysteretic model.

562 In this work, the strength reduction factor ($R$) of SDF oscillators which may be used to
563 quantify the structural inelastic seismic demand was examined. As schematically shown in
564 Fig. 19a, given a target ductility, the demand quantity was defined by the ratio of the
565 maximum force of the corresponding elastic SDF oscillator ($F_e$) to the yield force of the
566 self-centring oscillator ($F_y$). The demand quantity may be used to prescribe the strength
567 demand of the inelastic SDF system, and it can be computed using a
568 constant-ductility-based spectral analysis procedure [47-49]. As a sensitivity analysis, $\beta$ =
569 0.2 and 1.0 was utilised in this work, and $\alpha$ was varied from 0.05 to 0.75. To offer
570 insightful lights on SDF systems with varied dynamic characteristics, SDF systems with
571 period ranging from 0.1 s to 5.0 s were examined, and all the systems were assigned with a
572 unit mass. In the SDF models, the constant damping ratio of 0.05 was assumed. In this
573 study, 320 near-field earthquake motions with intense velocity pulses were compiled as
574 input excitations. The pseudo-acceleration spectra of these ground motions are

575 demonstrated in Fig. 19b. The detailed information about the earthquake motions can be
576 found in a companion work [49].
577
578 *4.3.2 Strength reduction factor demand and discussions*
579 Representative mean strength reduction factor spectra of the SDF systems with varied
580 hysteretic parameters are shown in Fig. 20. The statistic distribution of the strength
581 reduction factor in case of $\beta$ =1.0 are also indicated in the figure. In general, the mean
582 strength reduction factor increases with increasing ductility, indicating that the inelastic
583 strength demands of the system may be mitigated if systems are able to develop significant
584 inelastic deformations. This observation becomes evident when the post-yield stiffness
585 ratio is significant. It can also be observed that the mean strength reduction factor of
586 short-period systems rises when the post-yield stiffness ratio increases, confirming the
587 beneficial effect of a high post-yield stiffness ratio for mitigating the strength demand of
588 short-period systems. Concurrently, an increasing "flag height" (i.e. $\beta$) leads to increasing
589 strength reduction factor, and the inelastic seismic demands may also be mitigated. It is
590 worth noting that the effect of post-yield stiffness ratio on the strength reduction factors
591 and the dispersion properties was also in line with bilinear kinematic SDF systems
592 examined in the literature [50]. The feasibility of modulating the seismic demands of
593 flag-shaped SDF systems by adjusting the hysteretic parameters was also confirmed by
594 previous analyses [43].
595 Therefore, it may be necessary to re-emphasise the importance of the training protocol,
596 as it may contribute to modulating the structural hysteretic characteristics. This may be

apparent from comparison of the cyclic tension-release responses of specimen PB in "Phase 1" and "Phase 3". However, special cautions may need to be exercised since the self-centring deformation range of the SMA plates was limited. The heatmap of the strength reduction factor for the flag-shaped systems with $\beta$ = 1.0 is illustrated in Fig. 20, and it can be confirmed that an increasing ductility leads to increasing dispersion of the strength reduction factor, whereas an increasing post-yield stiffness ratio leads to the opposite trend. Thus, trained SMA plates with a high post-yield stiffness ratio contribute to stabilising the nonlinear dynamic responses of structures. In summary, it is affirmed that the inelastic seismic demands of the structures equipped with superelastic SMA plates may be appreciably affected by the cyclic performance of the SMA plates, and a trained SMA plate could lead to an increasing post-yield stiffness ratio, resulting in seismic responses of the systems with reduced dispersion. However, the enhanced post-yield stiffness also results in increasing strength of the SMA plates in the inelastic stage, and it needs to be careful when designing the surrounding elements to concentrate inelastic actions in the SMA element. In addition, training cycles also compromise the energy dissipation of SMA plates, and hence the energy dissipation of the structural system may be affected, which may further lead to an increase of inelastic seismic demands. Thus, practising engineers may make trade-offs depending on engineering judgment, and supplemental energy dissipation mechanism may be applied to enhance the energy dissipation capacity of structural systems.

## 5. Summary and conclusions

This research focused on the hysteretic performance and seismic applications of

commercial superelastic SMA plates, and the emphasis was given to cyclic tension-release behaviour of the SMA plates. The thermal characteristics, strength, post-yield behaviour, self-centring capacity and energy dissipation of a series of SMA plate specimens were carefully examined. In addition, the influence of training protocols on the cyclic tension-release behaviour of SMA plates was explored, and the mechanical characteristics of SMA plates before training and in the post-training stage were compared. Based on the test data of SMA plates, a detailed numerical modelling of an energy dissipation connection was developed and verified. The feasibility of applying cyclic tension-release behaviour of the SMA plates in seismic resistant structures was confirmed. The nonlinear dynamic analyses of single-degree-of-freedom (SDF) systems were also carried out to demonstrate the potential effect of the cyclic tension-release behaviour of SMA plates on inelastic seismic demands of structures. The main research findings are summarised as follows:

- Both normal and high strength SMA plates were able to develop encouraging recentring behaviour under cyclic tension-release loading scenarios in a reasonable deformation range, confirming their potential for seismic applications. For normal strength SMA plates, the specimens were able to recover 56% to 82% of the strain when loaded to 4% in Phase 1, and the high strength SMA plates could recover more than 90% of the deformation when loaded to 4%.
- For SMA plate specimens in “Phase 1” test, the equivalent martensite transformation strength (simplified by bilinear idealisation) generally decreased with increasing cycle numbers (i.e. strain amplitude). After experiencing training cycles, the opposite

correlation between the equivalent martensite transformation strength and strain amplitude was characterised at small strain levels.

- The training protocols were effective in stabilising the residual strain of the SMA plates, and the post-yield stiffness ratio of the SMA plates was increased under cyclic tension-release loading scenarios. Concurrently, the energy dissipation of SMA plates in the post-training stage was decreased.
- The superelastic SMA plates may be used to offer self-centring capacity and energy dissipation for the proposed energy dissipation beam-to-column connection. It was observed that the influence of the material mechanical characteristics on the hysteretic behaviour of the energy dissipation connections was evident, as confirmed by the difference between connections equipped with SMA plates before training and that in the post-training stage.
- The strength reduction factor of SDF systems representing low-to-medium rise structures equipped with SMA plates can shed lights on the effect of cyclic tension-release behaviour of SMA plates on inelastic seismic demands of structural systems, and it was further observed that trained SMA plates with increased post-yield stiffness ratio may contribute to mitigating the dispersion of the strength reduction factor. Nevertheless, the reduced energy dissipation due to the training protocols may result in increase of inelastic seismic demand of a structure, and cautions may need to be exercised in seismic design.

## Acknowledgments

This research is financially supported by the Research Grants Council of the Hong Kong Special Administrative Region, China with Grant No. PolyU 152096/19E and National Natural Science Foundation of China (Grant No. 51890902 and 51708197). The constructive comments by the two anonymous reviewers are sincerely appreciated. The corresponding author would like to thank the constant support from his beloved wife Siqin, his daughter Yutong and all his families, particularly in this hard period.

## References

[1] Okazaki T, Lignos DG, Midorikawa M, Ricles JM, Love J. Damage to steel buildings observed after the 2011 Tohoku-Oki earthquake. Earthq Spectra 2013; 29(S1): S219-S243.

[2] Ricles JM, Sause R, Garlock MM, Zhao C. Posttensioned seismic-resistant connections for steel frames. J Struct Eng 2001; 127(2): 113-121.

[3] Garlock MM, Ricles JM, Sause R. Experimental studies on full-scale posttensioned steel connections. J Struct Eng 2005; 131(3): 438-448.

[4] Garlock MM, Sause R, Ricles JM. Behavior and design of posttensioned steel frame systems. J Struct Eng 2007; 133(3): 389-399.

[5] Christopoulos C, Tremblay R, Kim HJ, Lacerte M. Self-centering energy dissipative bracing system for the seismic resistance of structures: Development and validation. J Struct Eng 2008; 134(1): 96-107.

[6] Lin YC, Sause R, Ricles JM. Seismic performance of steel self-centering, moment-resisting frame: Hybrid simulations under design basis earthquake. J Struct Eng 2013; 139(11): 1823-1832.

687 [7] Zhang AL, Zhang YX, Li R, Wang ZY. Cyclic behavior of a prefabricated self-centering
688 beam-column connection with a bolted web friction device. Eng Struct 2016; 111:
689 185-198.
690 [8] Desroches R, Smith B. Shape memory alloys in seismic resistant design and retrofit: A
691 critical review of their potential and limitations. J Earthq Eng 2004; 8(3): 415-429.
692 [9] Wilson JC, Wesolowsky MJ. Shape memory alloys for seismic response modification: A
693 state-of-the-art review. Earthq Spectra 2005; 21(2): 569-601.
694 [10] Song G, Ma N, Li HN. Applications of shape memory alloys in civil structures. Eng
695 Struct 2006; 28(9): 1266-1274.
696 [11] DesRoches R, McCormick J, Delemont M. Cyclic properties of superelastic shape
697 memory alloy wires and bars. J Struct Eng 2004; 130(1): 38-46.
698 [12] Ocel J, DesRoches R, Leon RT, Hess WG, Krumme R, Hayes JR, Sweeney S. Steel
699 beam-column connections using shape memory alloys. J Struct Eng 2004; 130(5):
700 732-740.
701 [13] Sepúlveda J, Boroschek R, Herrera R, Moroni O. Steel beam–column connection using
702 copper-based shape memory alloy dampers. J Constr Steel Res 2008; 64(4): 429-435.
703 [14] Ma H, Cho C, Wilkinson T. A numerical study on bolted end-plate connection using
704 shape memory alloys. Mater Struct 2008; 41(8): 1419-1426.
705 [15] Fang C, Yam MCH, Lam ACC, Xie L. Cyclic performance of extended end-plate
706 connections equipped with shape memory alloy bolts. J Constr Steel Res 2014; 94:
707 122-136.
708 [16] Yam MCH, Fang C, Lam ACC, Zhang Y. Numerical study and practical design of
709 beam-to-column connections with shape memory alloys. J Constr Steel Res 2015; 104:
710 177-192.
711 [17] Fang C, Yam MCH, Chan TM, Wang W, Yang X, Lin X. A study of hybrid self-centring

712 connections equipped with shape memory alloy washers and bolts. Eng Struct 2018;
713 164: 155-168.
714 [18] Speicher, MS. DesRoches R, Leon RT. Experimental results of a NiTi shape memory
715 alloy (SMA)-based recentering beam-column connection. Eng Struct 2011; 33(9):
716 2448-2457.
717 [19] Wang W, Chan T, Shao H, Chen Y. Cyclic behavior of connections equipped with NiTi
718 shape memory alloy and steel tendons between H-shaped beam to CHS column. Eng
719 Struct 2015; 88: 37-50.
720 [20] Wang W, Chan TM, Shao H. Seismic performance of beam–column joints with SMA
721 tendons strengthened by steel angles. J Constr Steel Res 2015; 109: 61-71.
722 [21] Adachi, Y, Unjoh, S. Development of shape memory alloy damper for intelligent bridge
723 systems. Smart Structures and Materials: Smart Systems for Bridges, Structures, and
724 Highways. International Society for Optics and Photonics, 1999; 3671: 31-42.
725 [22] Wang B, Zhu SY. Superelastic SMA U-shaped dampers with self-centering functions.
726 Smart Mater Struct 2018; 27(5): 055003.
727 [23] Wang B, Zhu S, Casciati F. Experimental study of novel self-centering seismic base
728 isolators incorporating superelastic shape memory alloys. J Struct Eng 2020; 146(7):
729 04020129.
730 [24] Wang B, Zhu S, Chen K, Huang J. Development of superelastic SMA angles as
731 seismic-resistant self-centering devices. Eng Struct 2020; 218: 110836.
732 [25] Moradi S, Alam MS. Feasibility study of utilizing superelastic shape memory alloy
733 plates in steel beam–column connections for improved seismic performance. J Intel Mat
734 Syst Str 2015; 26(4): 463-475.
735 [26] Moradi S, Alam MS. Feasible application of shape memory alloy plates in steel
736 beam-column connections. Structures Congress 2015; 2089-2100.

737 [27] Yang JG, Kim JW, Lee JH, Kang S, Pag DS. Energy dissipation capacity of an
738 unstiffened extended end-plate connection with a SMA plate. Int J Steel Struct 2016;
739 16(4): 1309-1317.
740 [28] Fang C, Zheng Y, Chen J, Yam MCH, Wang W. Superelastic NiTi SMA cables:
741 Thermal-mechanical behavior, hysteretic modelling and seismic application. Eng Struct
742 2019; 183: 533-549.
743 [29] Frick CP, Ortega AM, Tyber J, Maksound AEM, Maier HJ, Liu YN, Gall K. Thermal
744 processing of polycrystalline NiTi shape memory alloys, Mat Sci Eng A-Struct 2005;
745 405(1-2): 34-49.
746 [30] Tyber J,.McCormick J, Gall K, DesRoches R, Maier HJ, AE Abdel Maksoud.
747 Structural engineering with NiTi. I: Basic materials characterization, J Eng Mech 2007;
748 133(9): 1009-1018.
749 [31] McCormick J,.Tyber J, DesRoches R,.Gall K, Maier HJ. Structural engineering with
750 NiTi. II: Mechanical behavior and scaling, J Eng Mech 2007; 133 (9): 1019-1029.
751 [32] ASTM, A370, Standard test methods and definitions for mechanical testing of steel
752 products, American Society for Testing and Material, Philadelphia, PA, 2002.
753 [33] Rigamonti D, Nespoli A, Villa E, Passaretti F. Implementation of a constitutive model
754 for different annealed superelastic SMA wires with rhombohedral phase. Mech Mater
755 2017; 112: 88-100.
756 [34] Wang B, Zhu S. Cyclic tension-compression behavior of superelastic shape memory
757 alloy bars with buckling-restrained devices. Constr Build Mater 2018; 186: 103-113.
758 [35] Miyazaki S, Imai T, Igo Y, Otsuka K. Effect of cyclic deformation on the
759 pseudoelasticity characteristics of Ti-Ni alloys. Metall Trans A 1986; 17(1): 115-120.
760 [36] Fang C, Yam MCH, Ma H, Chung KF. Tests on superelastic Ni-Ti SMA bars under
761 cyclic tension and direct-shear: towards practical recentring connections. Mater Struct

762 2015; 48(4): 1013-1030.
763 [37] McCormick J, DesRoches R. The effect of training, pre-straining, and loading history
764 on the properties of NiTi shape memory alloys for protective systems in civil structures.
765 Structures Congress 2006: Structural Engineering and Public Safety 2006; 1-10.
766 [38] Dolce M, Cardone D. Mechanical behaviour of shape memory alloys for seismic
767 applications 1. Martensite and austenite NiTi bars subjected to torsion. Int J Mech Sci
768 2001; 43(11): 2631-2656.
769 [39] Zhang AL, Zhang H, Jiang ZQ, Li C, Liu XC. Low cycle reciprocating tests of
770 earthquake-resilient prefabricated column-flange beam-column joints with different
771 connection forms. J Constr Steel Res 2020; 164: 105771.
772 [40] Jiang ZQ, Yang XF, Dou C, Li C, Zhang AL. Cyclic testing of replaceable damper:
773 Earthquake-resilient prefabricated column-flange beam-column joint. Eng Struct 2019;
774 183: 922-936.
775 [41] ABAQUS Analysis User's Manual. ABAQUS Standard, Version 6.12; 2012.
776 [42] Auricchio F, Coda A, Reali A, Urbano M. SMA numerical modeling versus
777 experimental results: parameter identification and model prediction capabilities. J
778 Mater Eng Perform 2009; 18(5-6): 649-654.
779 [43] Christopoulos C, Filiatrault A, Folz B. Seismic response of self-centring hysteretic
780 SDOF systems. Earthq Eng Struct Dyn 2002; 31(5): 1131-1150.
781 [44] Zhang C, Steele TC, Wiebe LDA. Design-level estimation of seismic displacements for
782 self-centering SDOF systems on stiff soil. Eng Struct 2018; 177: 431-443.
783 [45] Zhou Y, Song G, Huang S, Wu H. Input energy spectra for self-centering SDOF systems.
784 Soil Dyn Earthq Eng 2019; 121: 293-305.
785 [46] Qiu CX, Zhu S. Performance-based seismic design of self-centering steel frames with
786 SMA-based braces. Eng Struct 2017; 130: 67-82.

[47] Ke K, Yam MCH, Zhang H, Lam ACC, Zhou X. High strength steel frames with SMA connections in self-centring energy dissipation bays: behaviour insights and a multi-mode-based nonlinear static procedure. Smart Mater Struct 2020; 29(12): 125020.

[48] Leelataviwat S, Saewon W, Goel SC. Application of energy balance concept in seismic evaluation of structures. J Struct Eng 2009; 135(2): 113-121.

[49] Zhang R, Wang W, Ke K. Quantification of seismic demands of damage-control tension-only concentrically braced steel beam-through frames (TCBSBFs) subjected to near-fault ground motions based on the energy factor. Soil Dyn Earthq Eng 2020; 129: 105910.

[50] Ke K, Yam MCH, Ke S. A dual-energy-demand-indices-based evaluation procedure of damage-control frame structures with energy dissipation fuses. Soil Dyn Earthq Eng 2017; 95: 61-82.

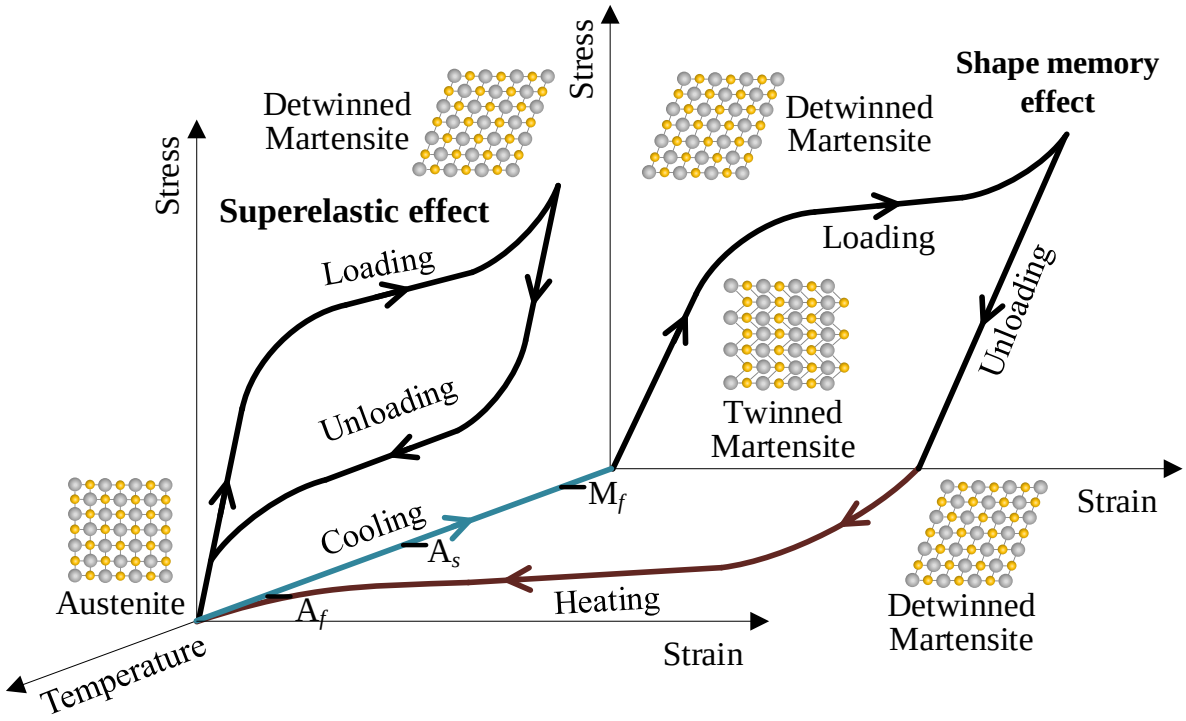


(a)

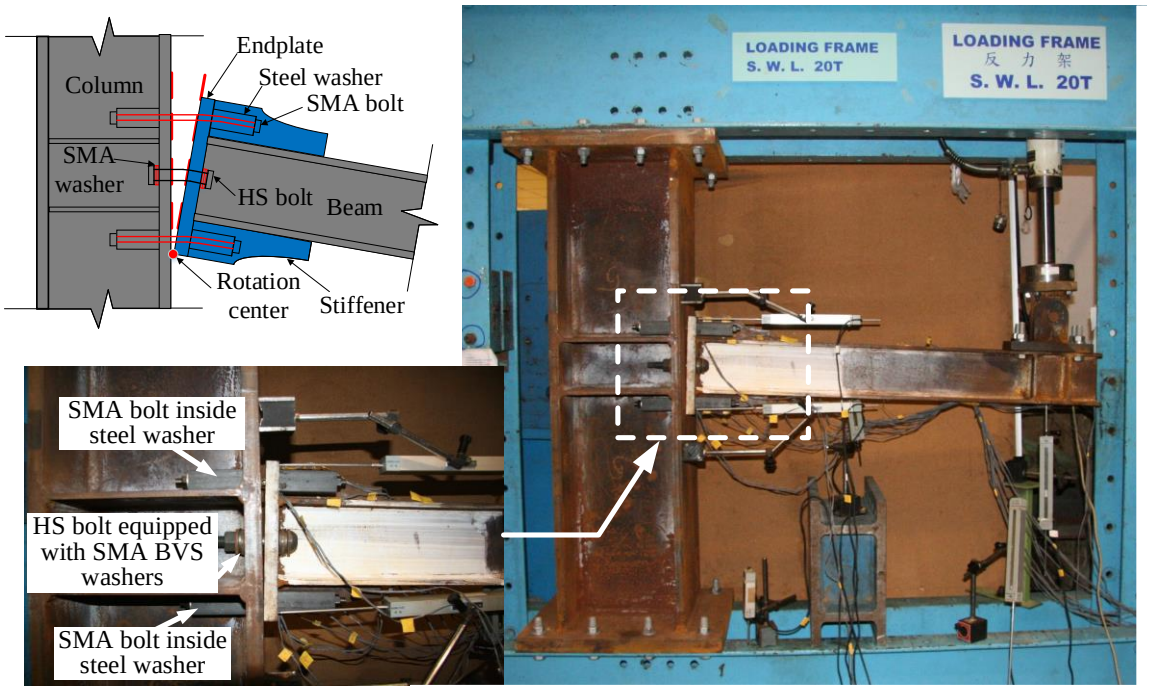


(b)

Fig. 1 Thermal-mechanical characteristics of SMA and novel SMA connections: (a) shape memory effect (SME) and superelastic effect (SE) and (b) typical connections equipped with SMAs [17].

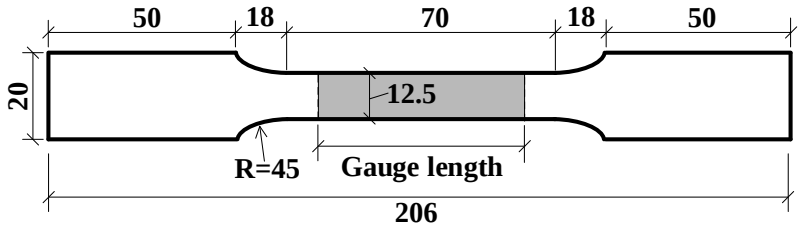


(a)

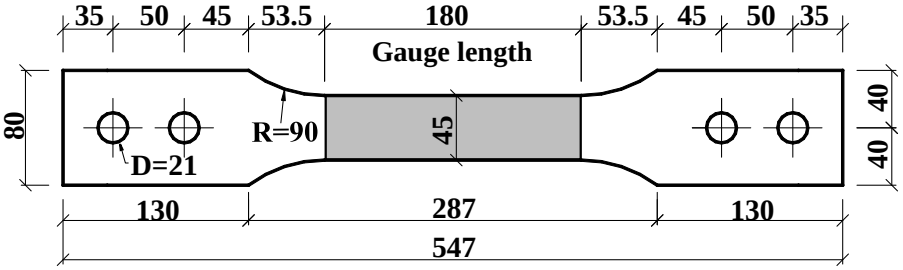


(b)

Fig. 2 SMA plate specimens: (a) Type A specimen and (b) Type B specimen.

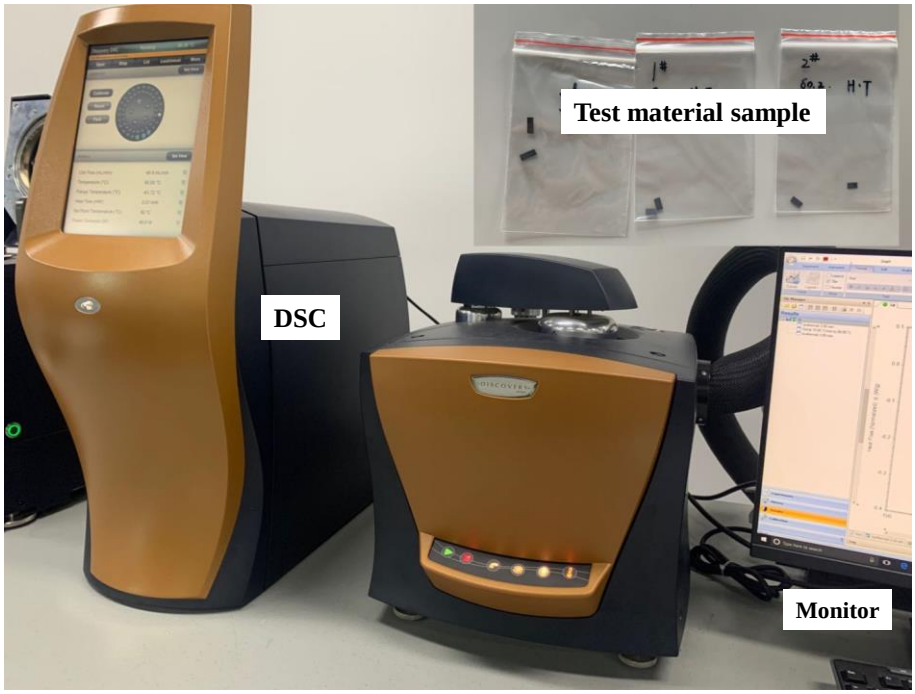


Fig. 3 Differential scanning calorimeter and SMA samples.

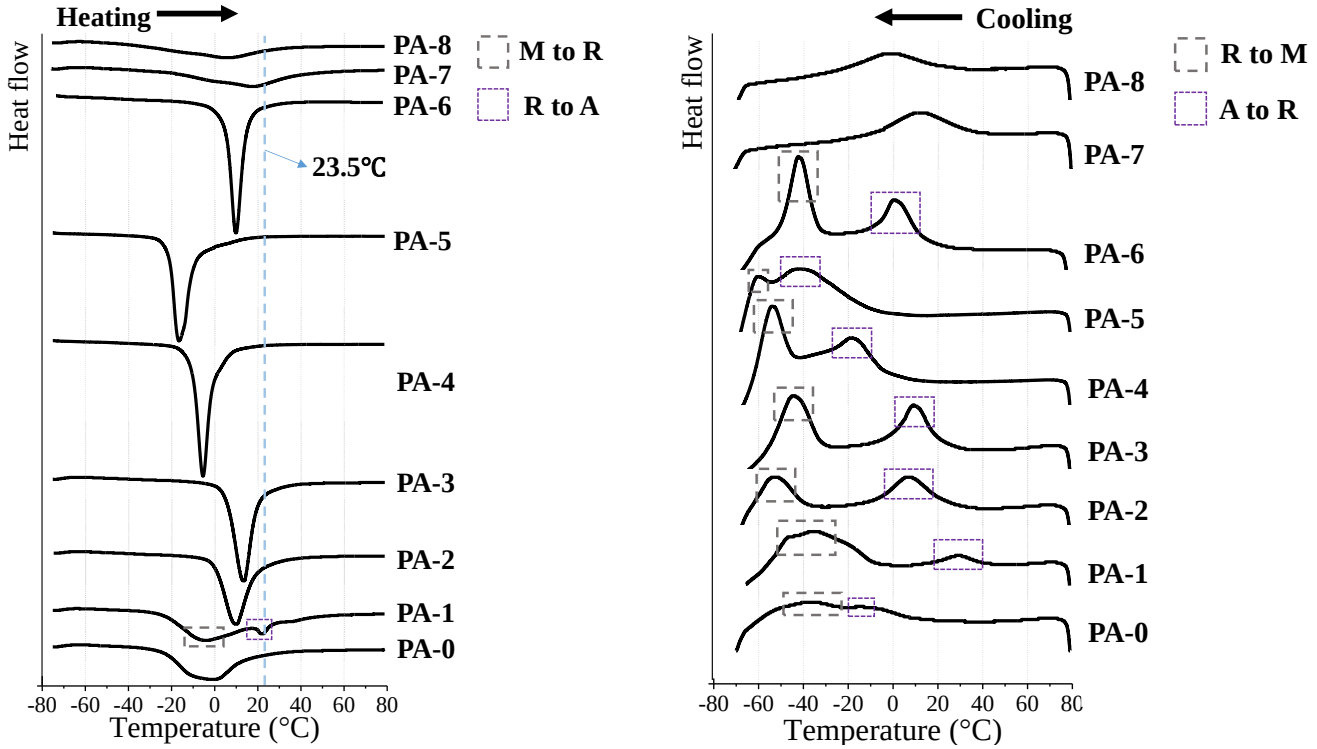


(a)

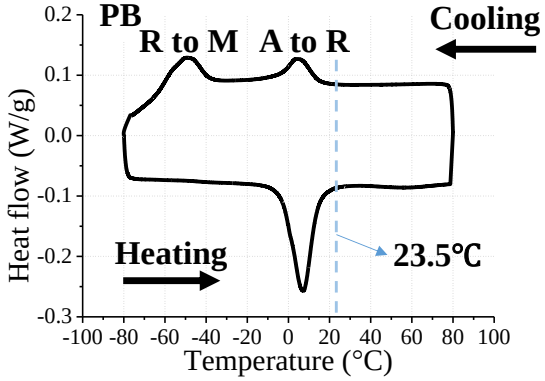


(b)

Fig. 4 Differential scanning calorimeter test results: (a) Type A specimens and (b) Type B specimen.

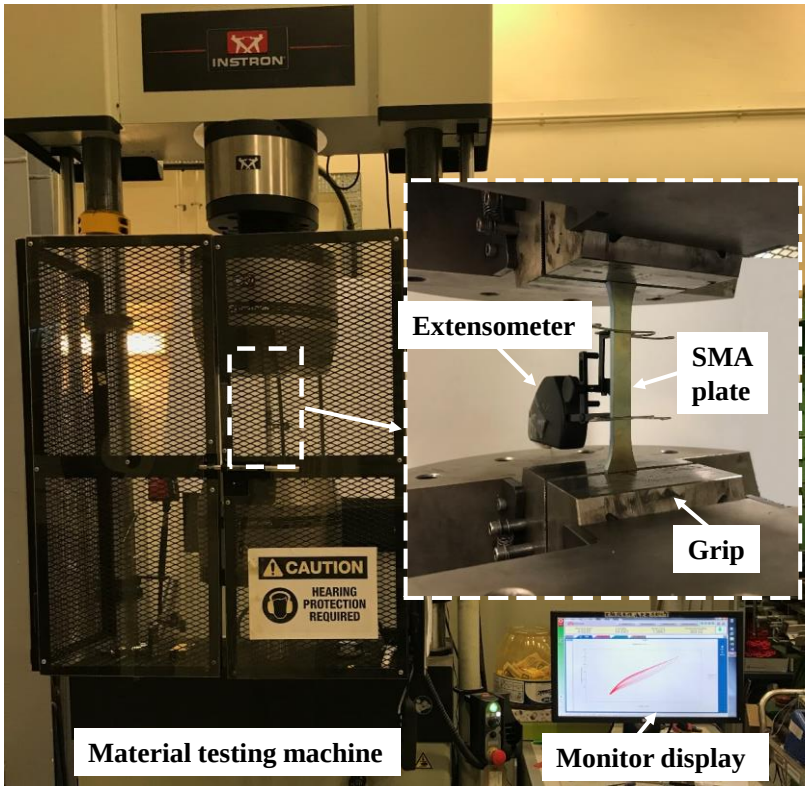


Fig. 5 Test arrangement.

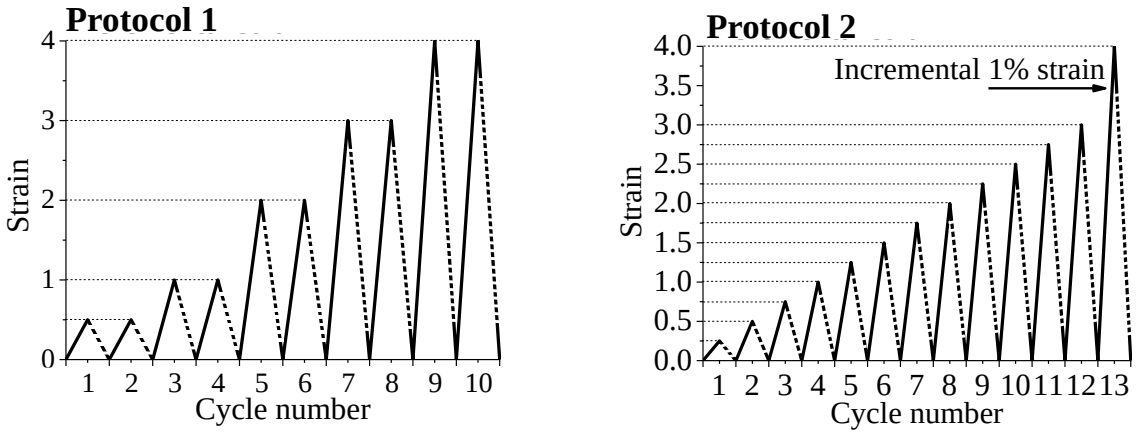


(a) (b)

Fig. 6 Loading protocol: (a) Protocol 1 and (b) Protocol 2.

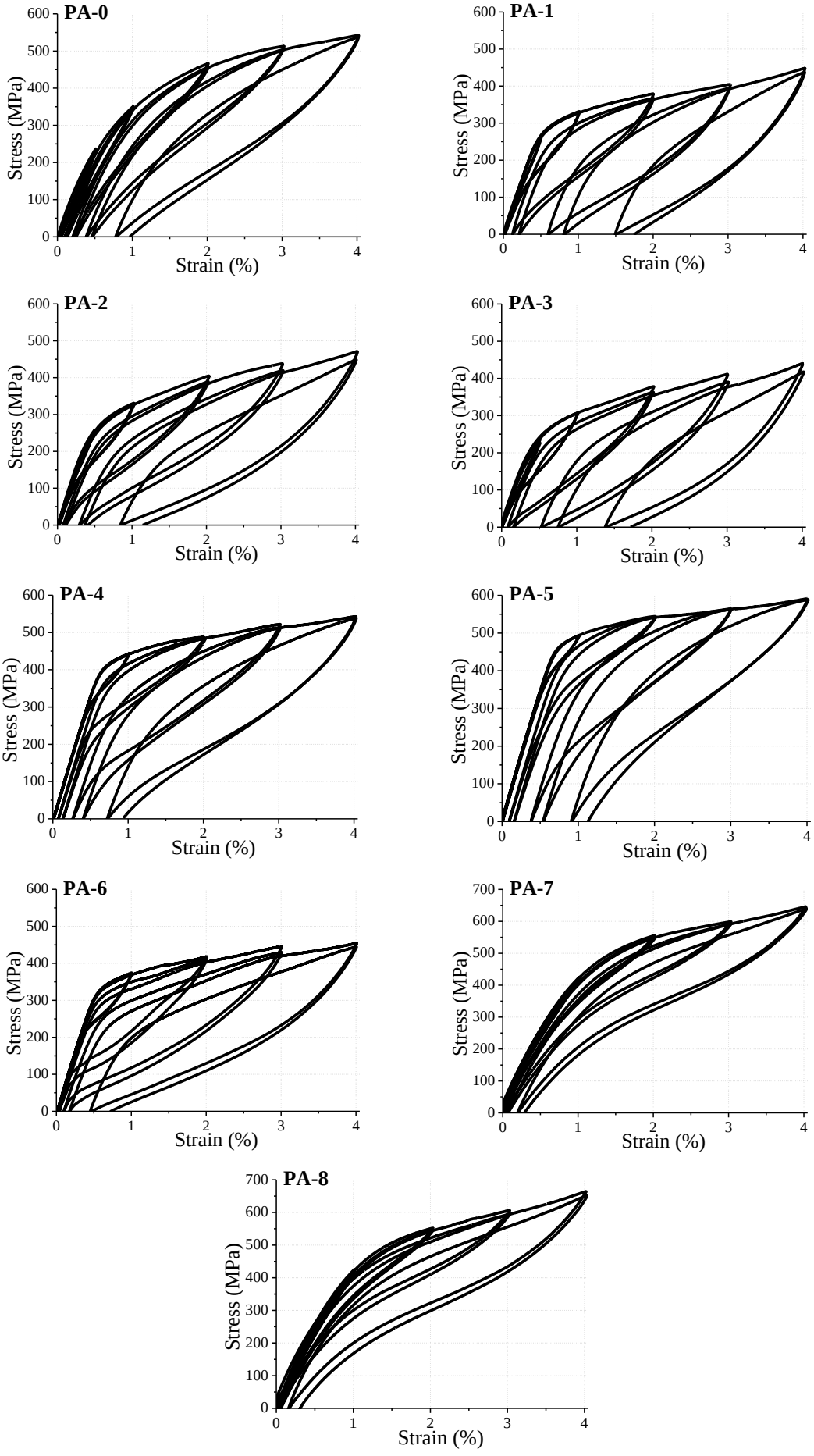


(a)

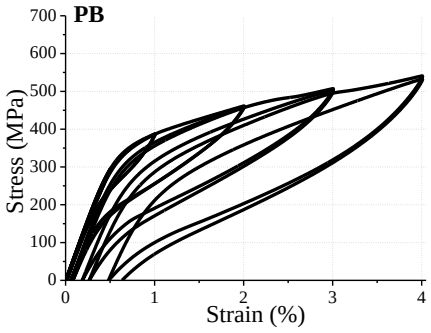


(b)

Fig. 7 Stress-strain responses (Phase 1 test): (a) Type A specimens and (b) Type B specimen.

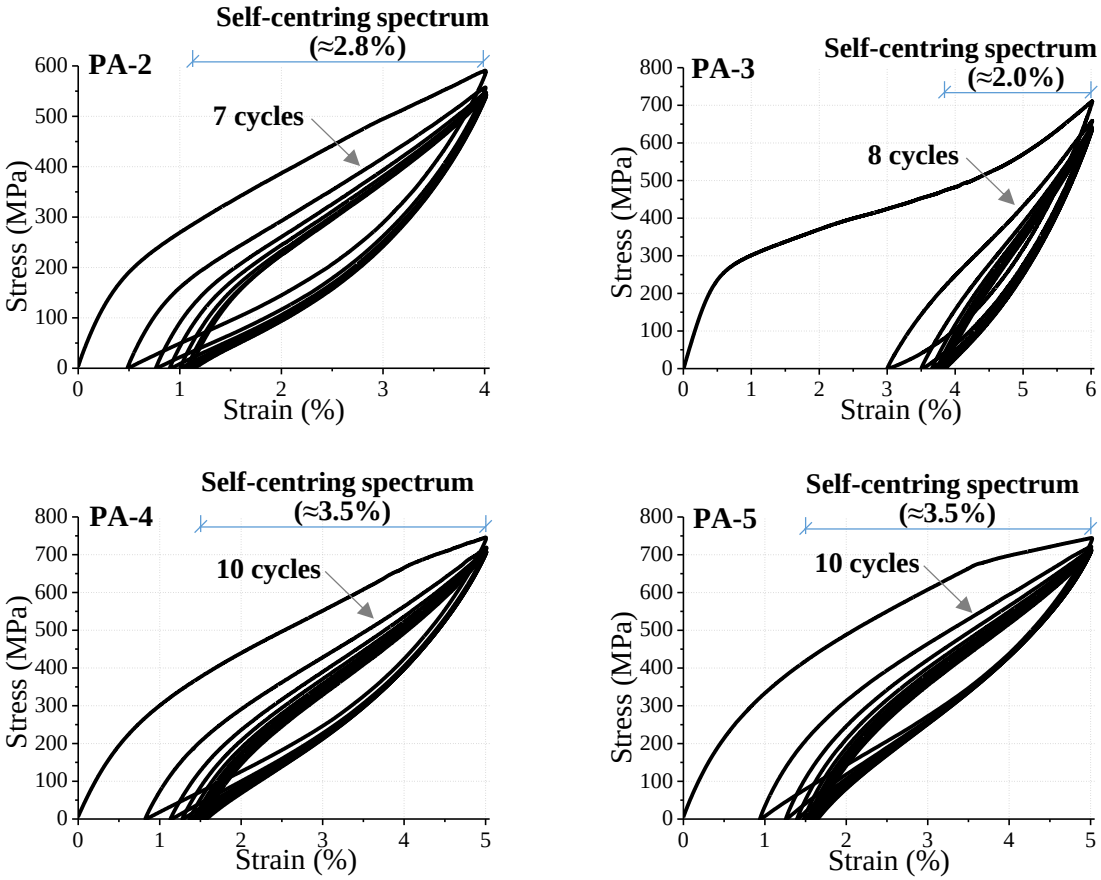


(a)

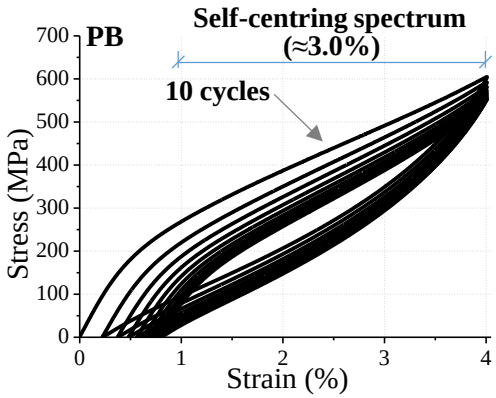


(b)

Fig. 8 Training cycles (Phase 2 test): (a) Type A specimens and (b) Type B specimen.

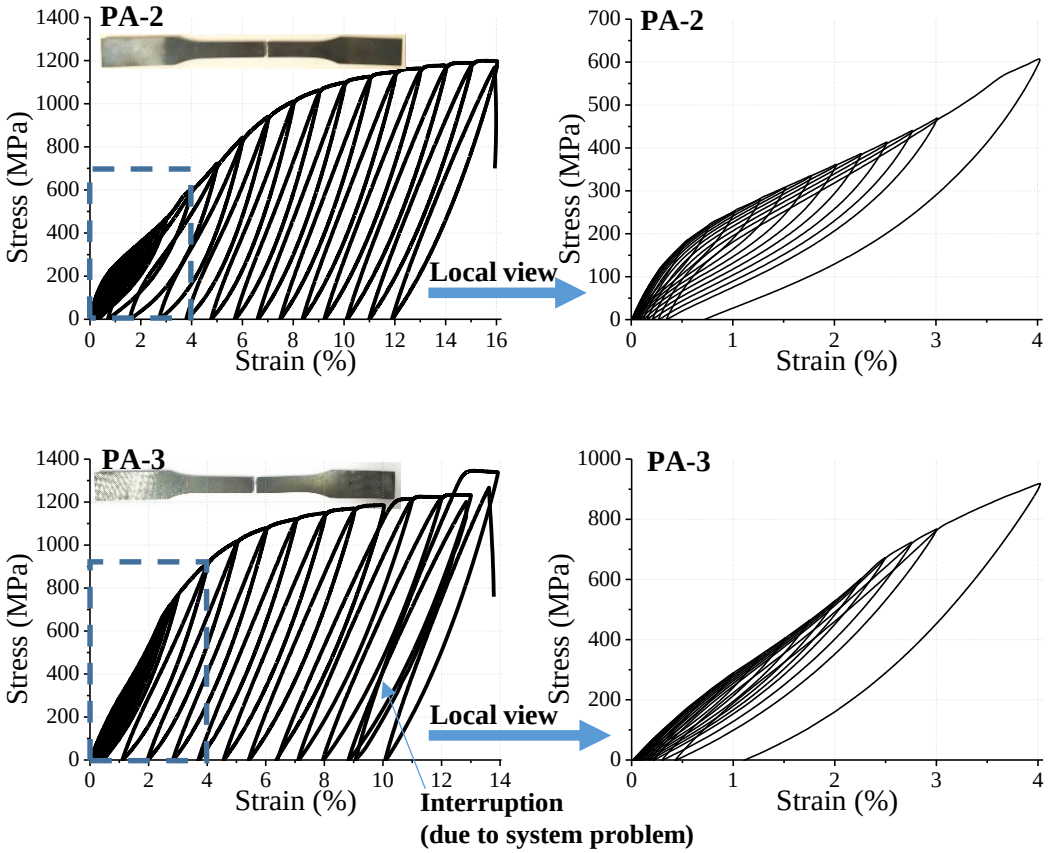


(a)

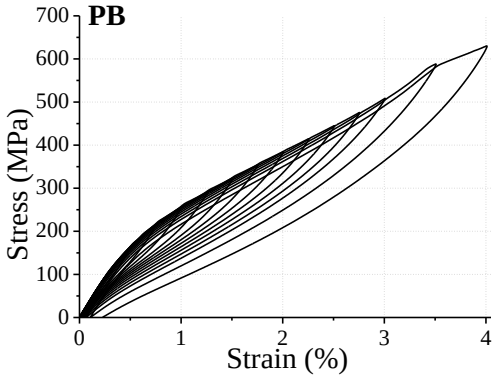


(b)

Fig. 9 Hysteretic responses of SMA plates after training (Phase 3 test): (a) Type A specimens and (b) Type B specimen.

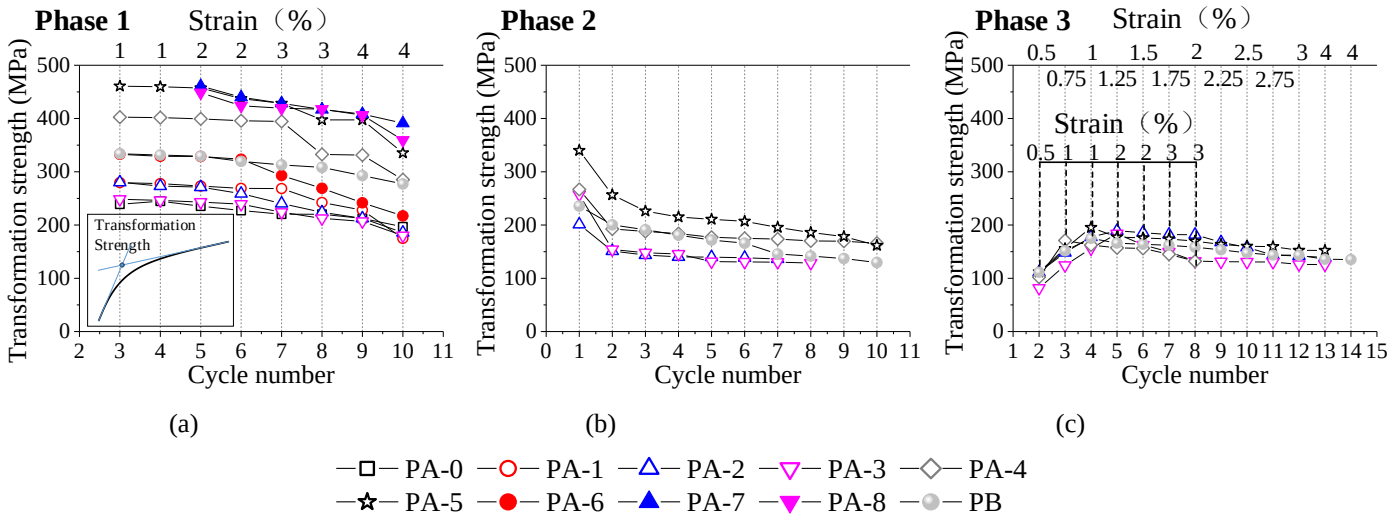


Fig. 10 Equivalent martensite transformation strength: (a) Phase 1, (b) Phase 2 and (c) Phase 3.

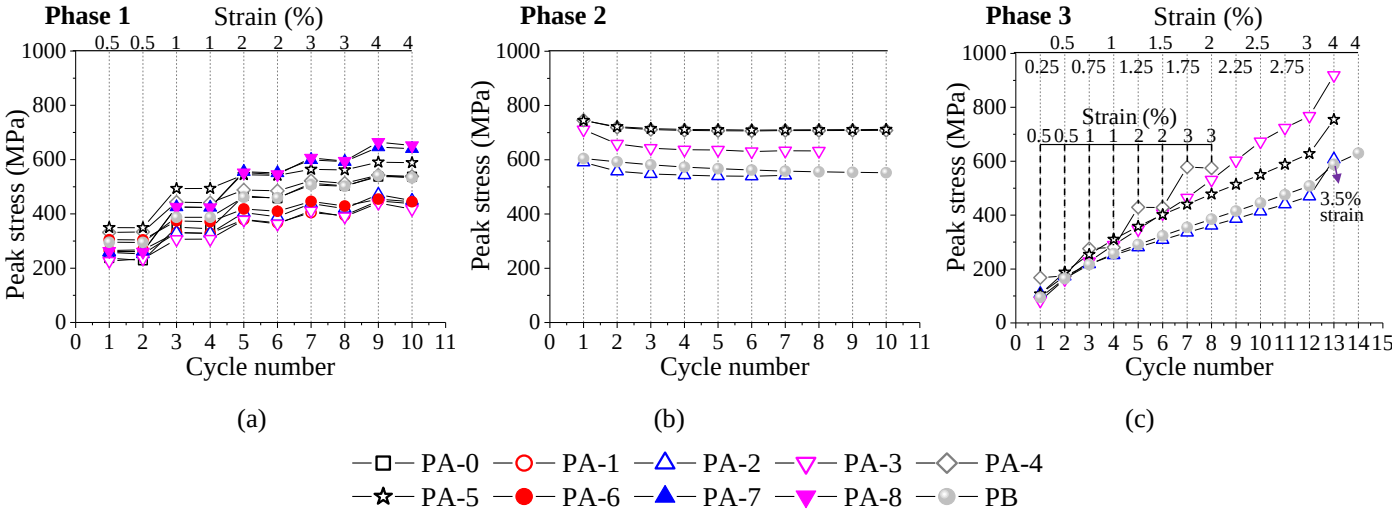


Fig. 11 Peak strength: (a) Phase 1, (b) Phase 2 and (c) Phase 3.

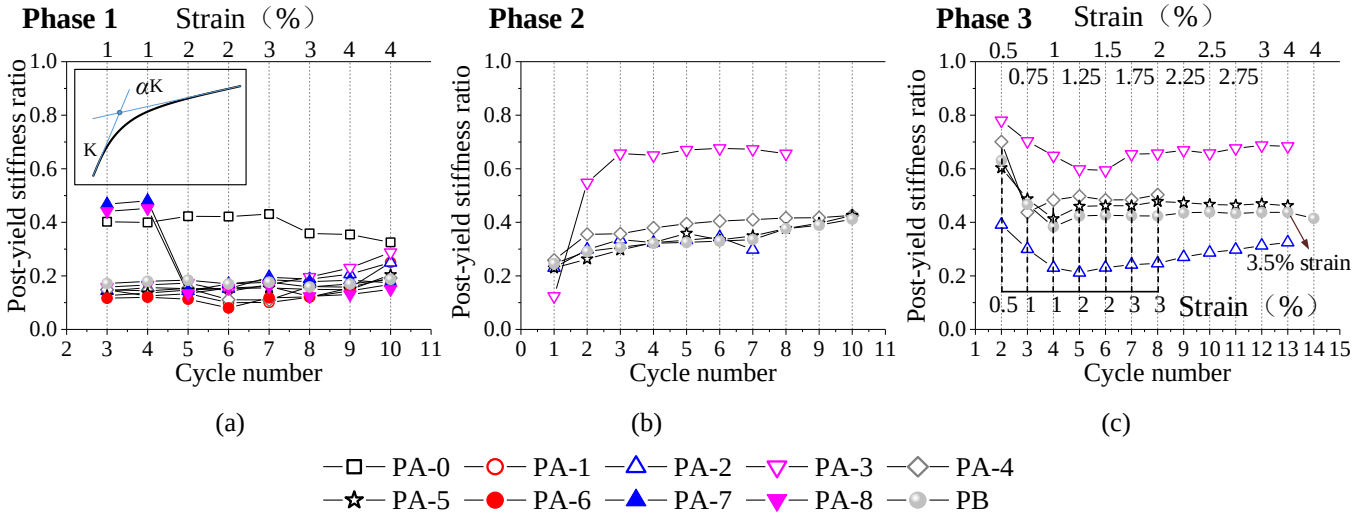


Fig. 12 Post-yield stiffness ratio: (a) Phase 1, (b) Phase 2 and (c) Phase 3.

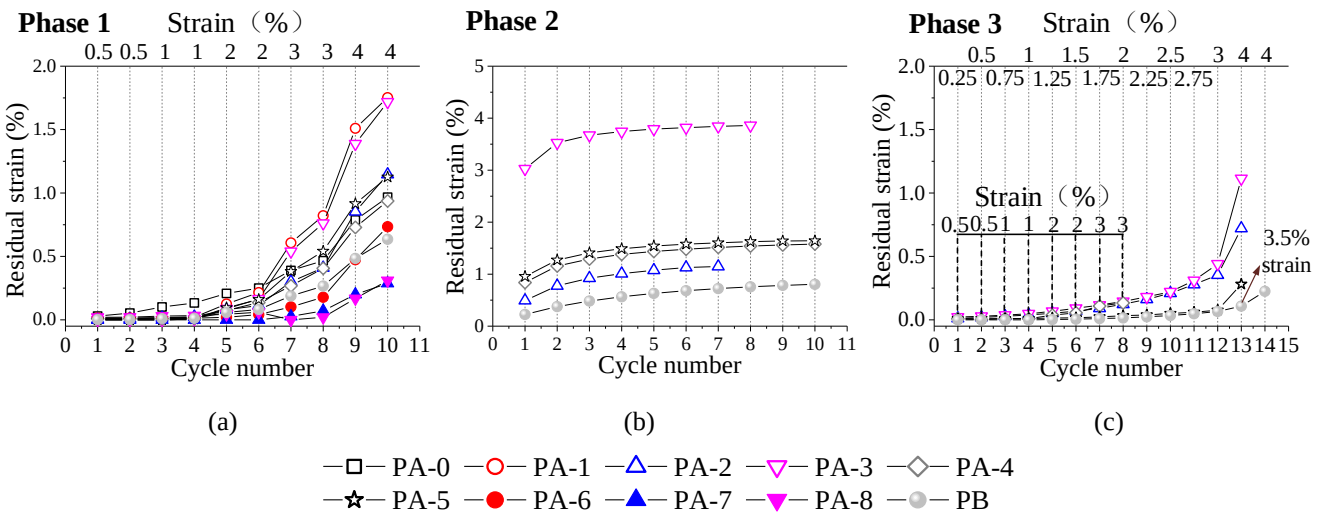


Fig. 13 Residual strain: (a) Phase 1, (b) Phase 2 and (c) Phase 3.

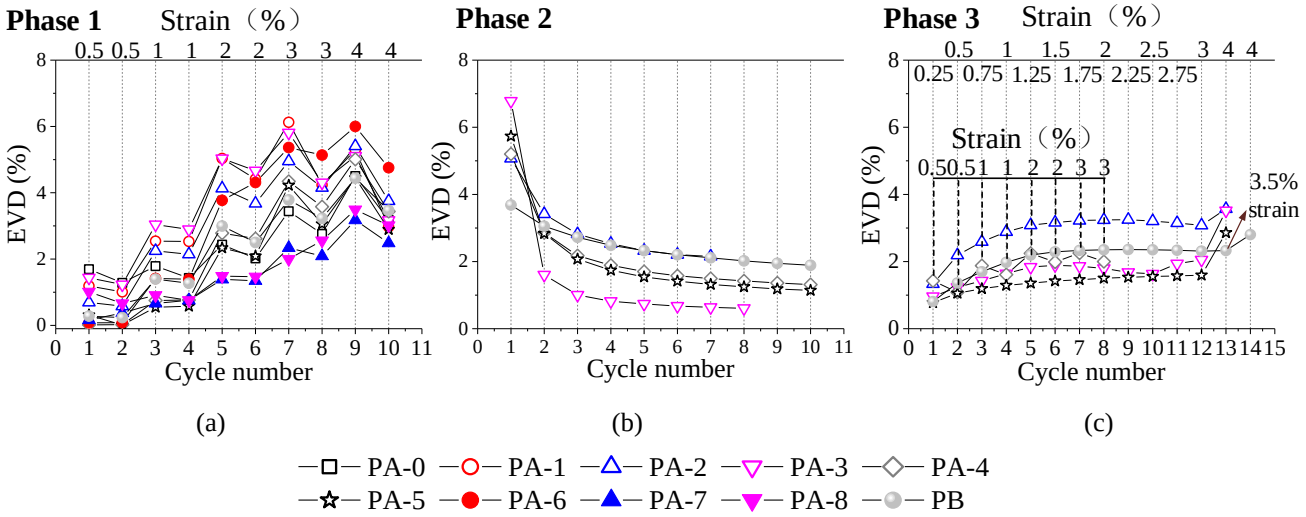


Fig. 14 Equivalent viscous damping: (a) Phase 1, (b) Phase 2 and (c) Phase 3.

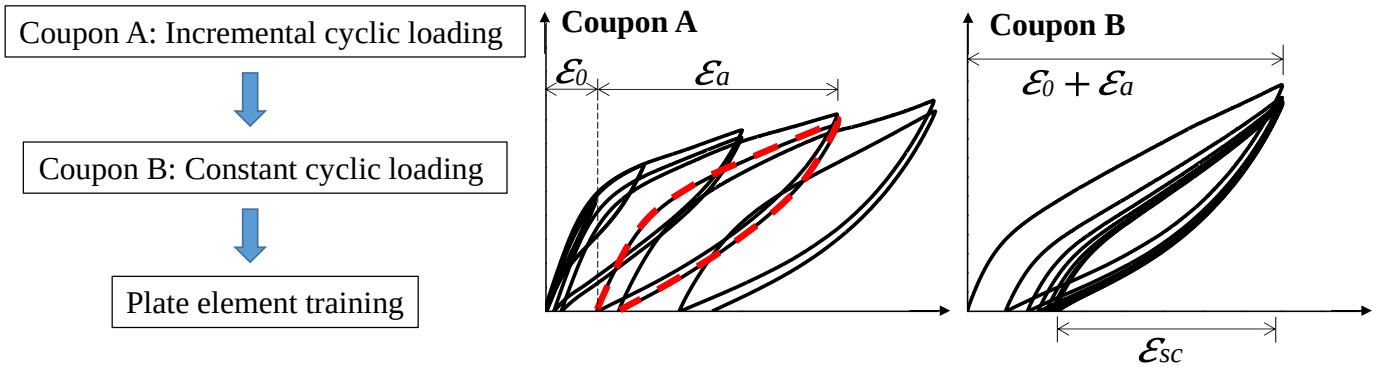


Fig. 15 Flowchart for training the SMA plate element under cyclic tension-release scenarios.

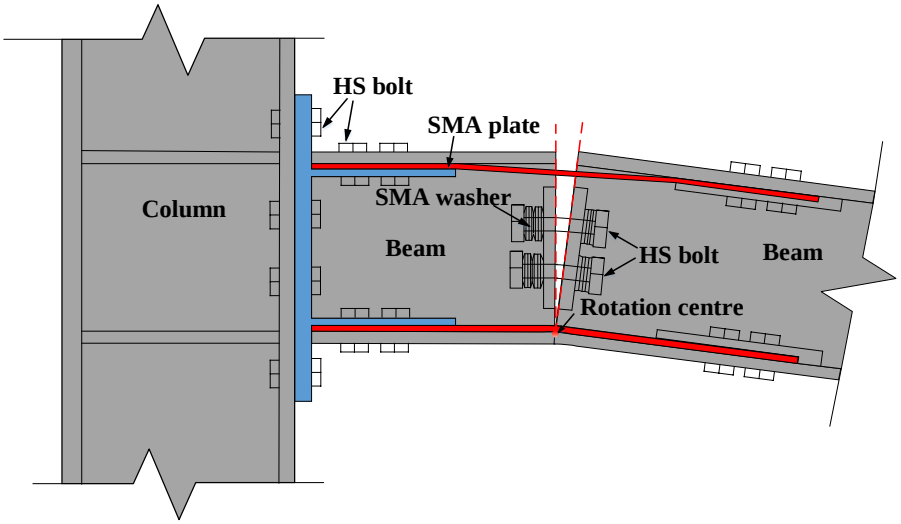


Fig. 16 Concept of the proposed connection.

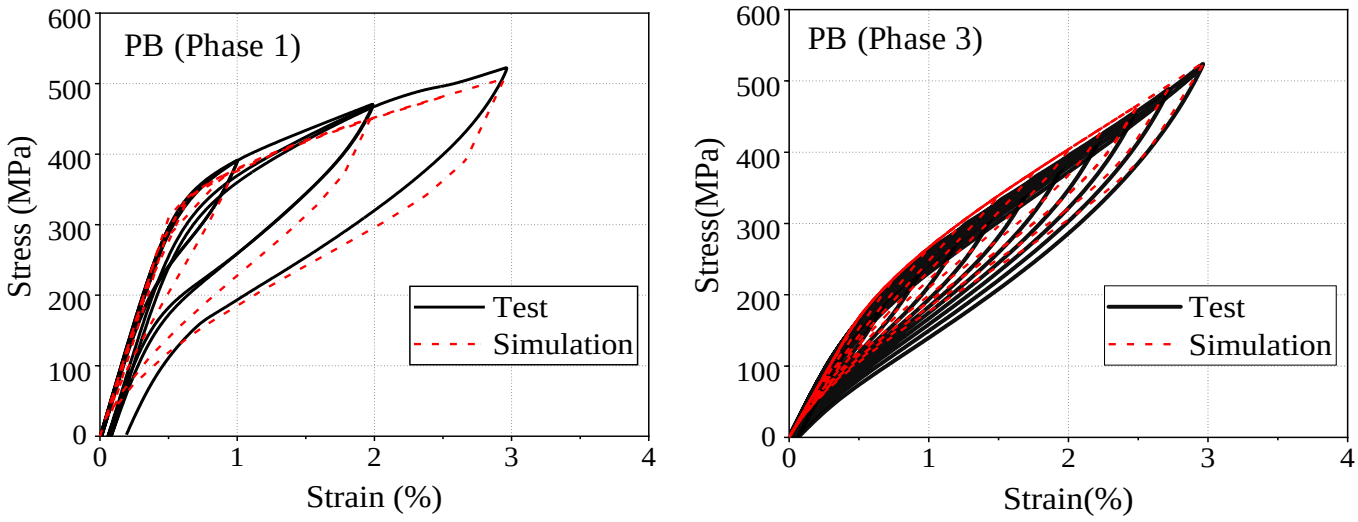


(a)

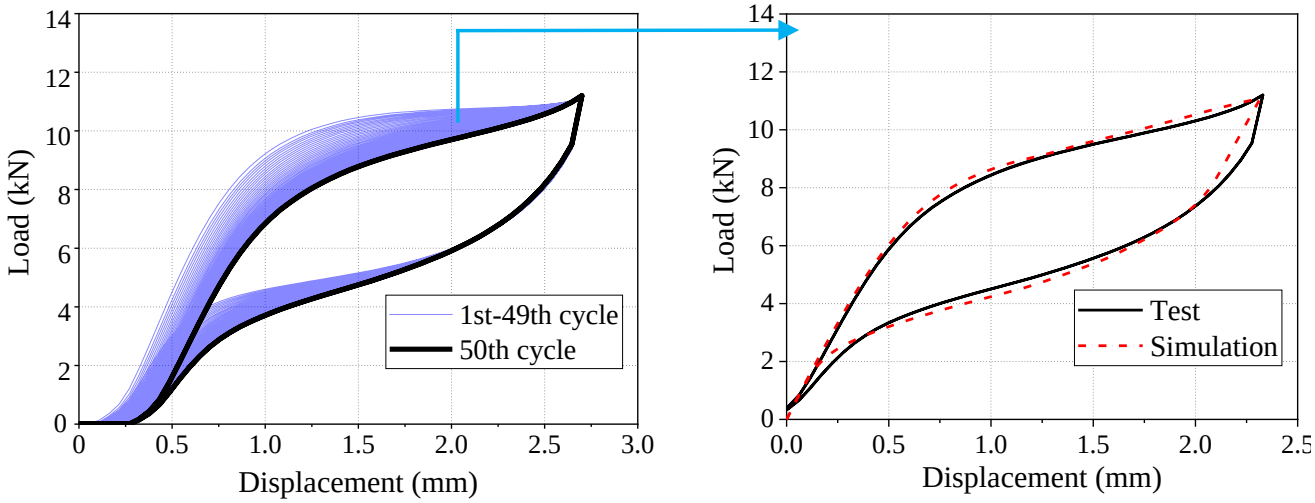


(b)

Fig. 17 FE modelling of the SMA elements: (a) SMA plates and (b) SMA washers [17].

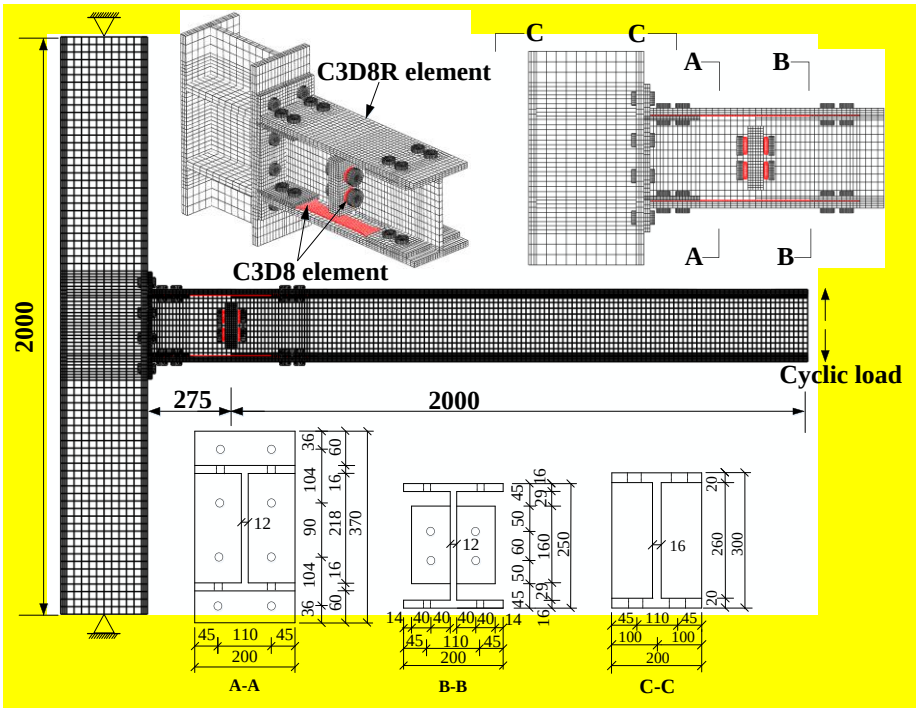
C3D8R element
C3D8 element
C
C
A
B
A
B
2000
Cyclic load
275
2000
12
16
A-A
B-B
C-C

(a)

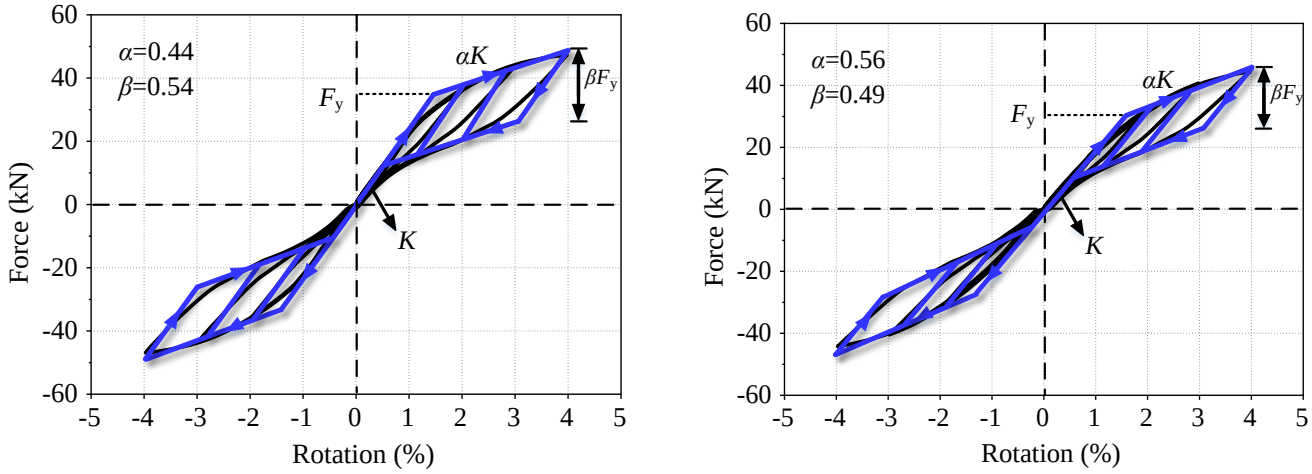
α=0.44
β=0.54
αK
βF_y
F_y
K
Force (kN)
Rotation (%)
α=0.56
β=0.49
αK
βF_y
F_y
K
Force (kN)
Rotation (%)

(b)

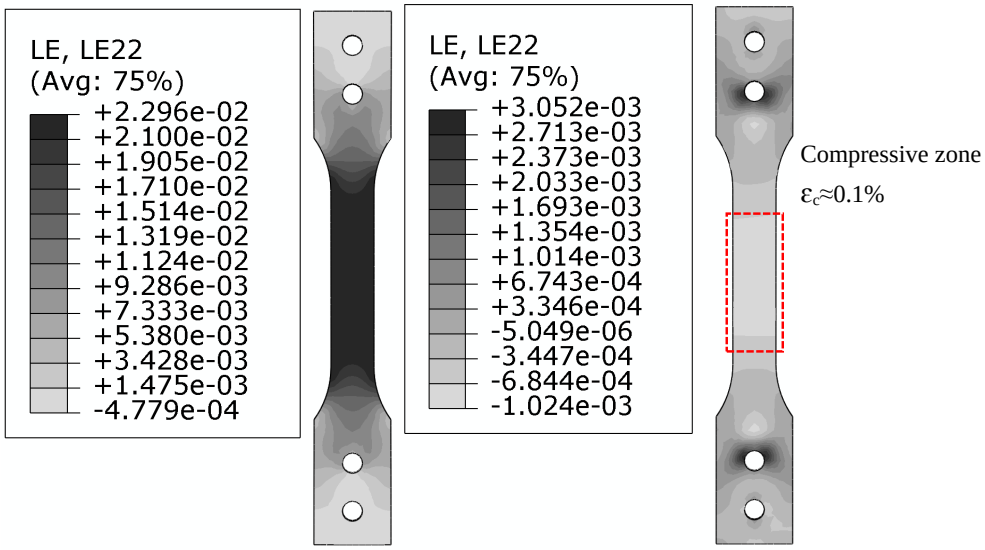
LE, LE22
(Avg: 75%)
+2.296e-02
+2.100e-02
+1.905e-02
+1.710e-02
+1.514e-02
+1.319e-02
+1.124e-02
+9.286e-03
+7.333e-03
+5.380e-03
+3.428e-03
+1.475e-03
-4.779e-04
LE, LE22
(Avg: 75%)
+3.052e-03
+2.713e-03
+2.373e-03
+2.033e-03
+1.693e-03
+1.354e-03
+1.014e-03
+6.743e-04
+3.346e-04
-5.049e-06
-3.447e-04
-6.844e-04
-1.024e-03
Compressive zone
ε_c≈0.1%

(c)

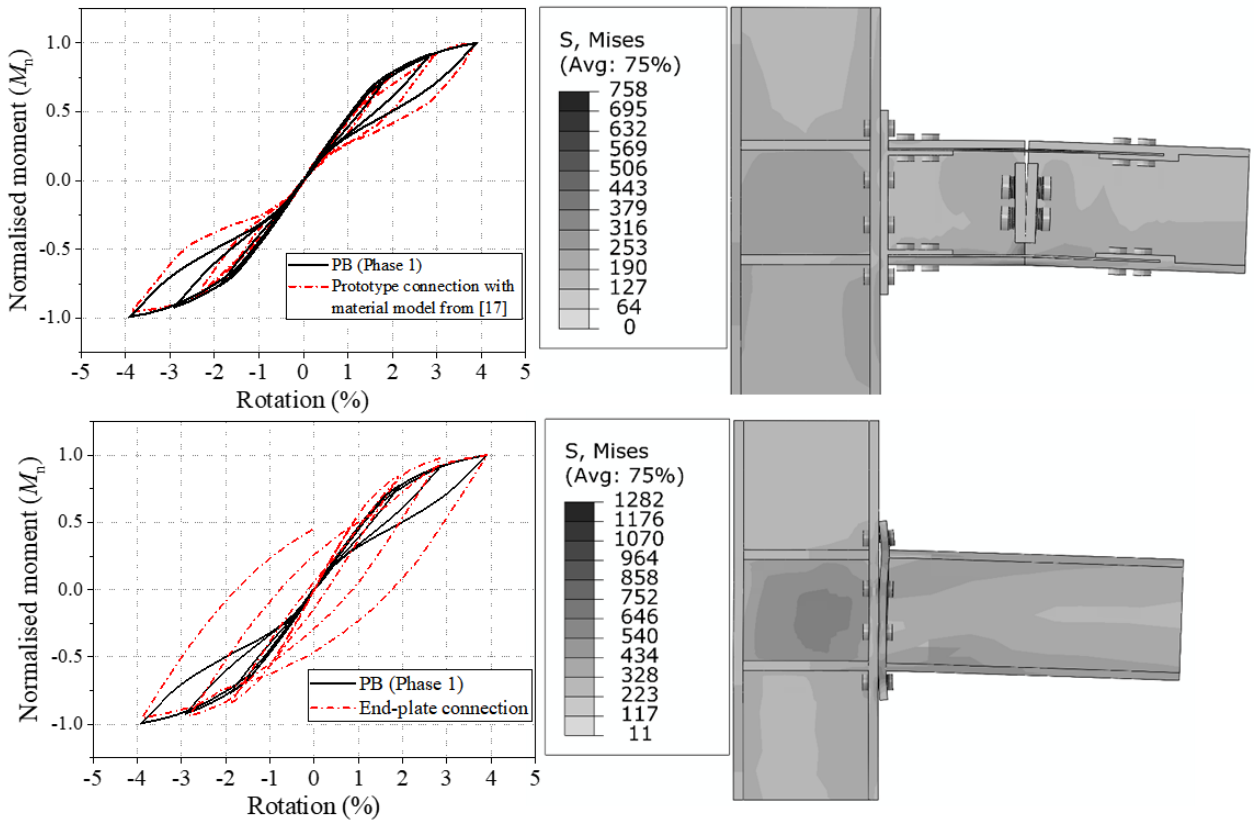


(d)

Fig. 18 Hysteretic responses of the prototype connection: (a) FE modelling, (b) hysteretic curves, (c) axial strain of the SMA plate and (d) comparisons with other connections.

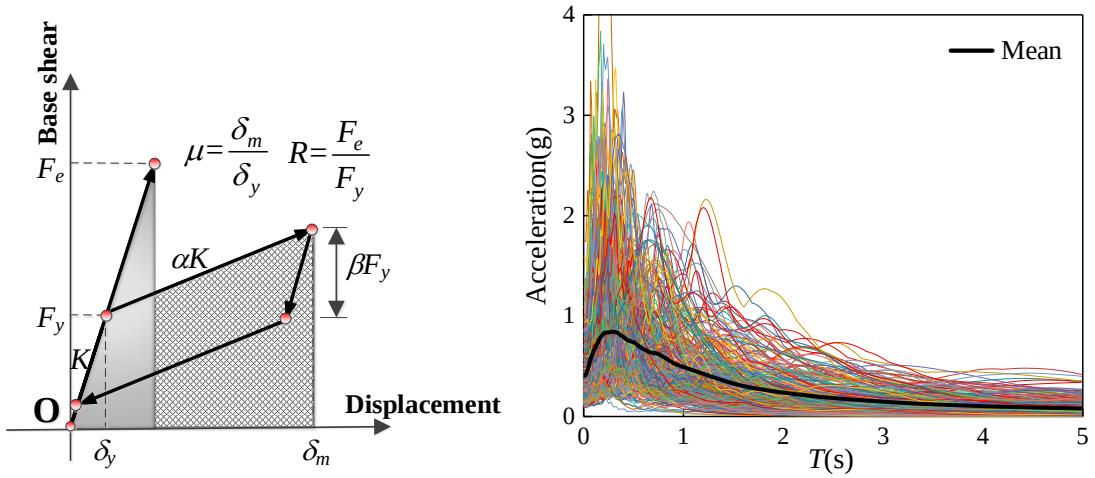


Fig. 19 Equivalent SDF systems and quantities: (a) SDF system and (b) earthquake ground motions.

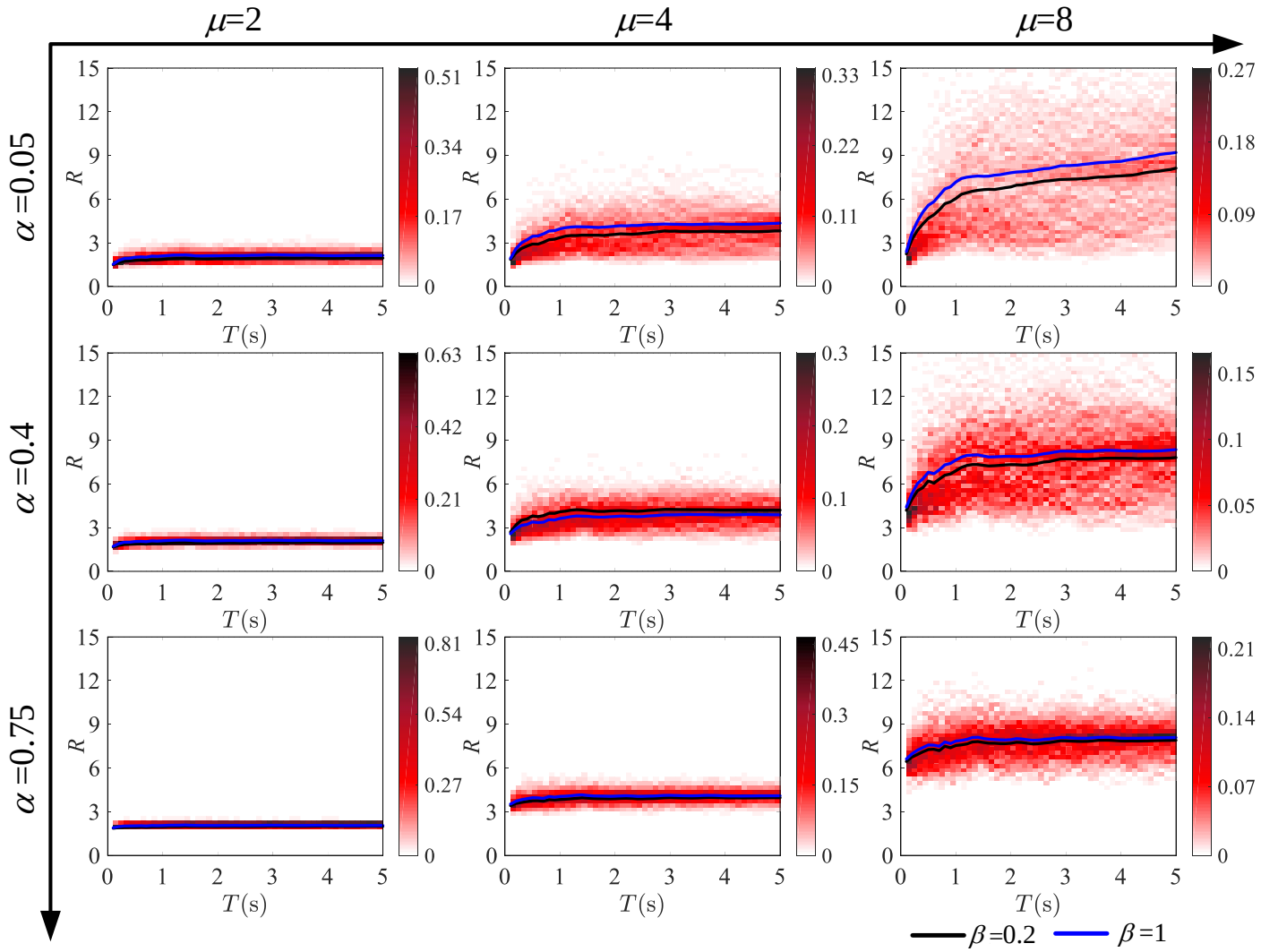


Fig. 20 Strength reduction factor spectra.

Table 1 SMA plate specimens.

| **Specimen label** | **Width of the gauge length (mm)** | **Plate thickness (mm)** | **Nominal $A_f$ (°C)** | **Specimen type** | **Loading protocol** |
|---|---|---|---|---|---|
| PA-0 | 12.51 | 4.11 | 14 | Type A | Phase 1 |
| PA-1 | 12.49 | 4.12 | 16 | Type A | Phase 1 |
| PA-2 | 12.34 | 4.17 | 16 | Type A | Phase 1+Phase 2+Phase 3 (**Protocol 2**) |
| PA-3 | 12.35 | 4.20 | 19 | Type A | Phase 1+Phase 2+Phase 3 **(Protocol 1)** |
| PA-4 | 11.73 | 4.23 | 13 | Type A | Phase 1+Phase 2+Phase 3 **(Protocol 2)** |
| PA-5 | 12.20 | 4.20 | 10 | Type A | Phase 1+Phase 2+Phase 3 **(Protocol 2)** |
| PA-6 | 12.31 | 4.16 | 12 | Type A | Phase 1 |
| PA-7 | 12.48 | 4.19 | 14 | Type A | Phase 1 |
| PA-8 | 12.48 | 4.20 | 12 | Type A | Phase 1 |
| PB | 43.00 | 4.22 | 14 | Type B | Phase 1+Phase 2+Phase 3 **(Modified Protocol 2)** |

Table 2 SMA material properties in FE analyses.

| Mechanical quantities | PB (Phase 1) | PB (Phase 3) | SMA washer |
|---|---|---|---|
| Forward transformation start stress $\sigma^{MS}$ | 300 MPa | 140 MPa | 300 MPa |
| Forward transformation end stress $\sigma^{Mf}$ | 750 MPa | 700 MPa | 500 MPa |
| Reverse transformation start stress $\sigma^{AS}$ | 420 MPa | 420 MPa | 250 MPa |
| Reverse transformation end stress $\sigma^{Af}$ | 0 MPa | 0 MPa | 75 MPa |
| Austenite elasticity $E^A$ | 63 GPa | 35 GPa | 40 GPa |
| Martensite elasticity $E^M$ | 31 GPa | 30 GPa | 100 GPa |
| Poisson's Ratio $v^A$ | 0.33 | 0.33 | 0.33 |
| Poisson's Ratio $v^M$ | 0.33 | 0.33 | 0.33 |

Table 3 Information about the prototype connections.

| Member | Section | Dimension (mm) | Steel grade |
|---|---|---|---|
| Column | H300×200×16×20 | $Lc$=2000 | Q460 |
| Beam 1 | H250×200×12×16 | $L_B$=2000 | Q460 |
| Beam 2 | H250×200×12×16 | $L_B$=275 | Q460 |

## Conflict of Interest

There is no financial/personal interest or belief that could affect our objectivity. There are no potential conflicts of interest either.

## Author statement

**Xuhong Zhou:** Conceptualization, Writing-Reviewing and Editing, Investigation, Funding acquisition
**Ke Ke***: Software, Methodology, Validation, Formal analysis, Writing- Original draft preparation
**Michael CH Yam**: Writing-Reviewing and Editing, Supervision, Funding acquisition
**Qingyang Zhao:** Visualization, Investigation,
**Yun Huang:** Formal analysis (assistance), Writing-Reviewing and Editing
**Jin Di:** Investigation, Resources, Project administration